



## Rhenium–osmium isotope and highly-siderophile-element abundance systematics of angrite meteorites

Amy J.V. Riches<sup>a,\*</sup>, James M.D. Day<sup>b,c</sup>, Richard J. Walker<sup>c</sup>, Antonio Simonetti<sup>d</sup>, Yang Liu<sup>a</sup>, Clive R. Neal<sup>d</sup>, Lawrence A. Taylor<sup>a</sup>

<sup>a</sup> Planetary Geosciences Institute, Department of Earth and Planetary Sciences, University of Tennessee, Knoxville, TN 37966, United States

<sup>b</sup> Geosciences Research Division, Scripps Institution of Oceanography, La Jolla, CA 92093-0244, United States

<sup>c</sup> Department of Geology, University of Maryland, College Park, MD 20742, United States

<sup>d</sup> Department of Civil and Environmental Engineering and Earth Sciences, 156 Fitzpatrick Hall, University of Notre Dame, Notre Dame, IN 46556, United States

### ARTICLE INFO

#### Article history:

Received 24 February 2012

Received in revised form

17 July 2012

Accepted 8 August 2012

Editor: T. Elliott

Available online 15 September 2012

#### Keywords:

angrites  
osmium isotopes  
highly-siderophile-elements  
planetary differentiation  
impact processes  
late accretion

### ABSTRACT

Coupled  $^{187}\text{Os}/^{188}\text{Os}$  compositions and highly-siderophile-element (HSE: Os, Ir, Ru, Pt, Pd, and Re) abundance data are reported for eight angrite achondrite meteorites that include quenched- and slowly-cooled textural types. These data are combined with new major- and trace-element concentrations determined for bulk-rock powder fractions and constituent mineral phases, to assess angrite petrogenesis. Angrite meteorites span a wide-range of HSE abundances from  $< 0.005$  ppb Os (e.g., Northwest Africa [NWA] 1296; Angra dos Reis) to  $> 100$  ppb Os (NWA 4931). Chondritic to supra-chondritic  $^{187}\text{Os}/^{188}\text{Os}$  (0.1201–0.2127) measured for Angra dos Reis and quenched-angrites correspond to inter- and intra-sample heterogeneities in Re/Os and HSE abundances. Quenched-angrites have chondritic-relative rare-earth-element (REE) abundances at  $10\text{--}15 \times$  CI-chondrite, and their Os-isotope and HSE abundance variations represent mixtures of pristine uncontaminated crustal materials that experienced addition ( $< 0.8\%$ ) of exogenous chondritic materials during or after crystallization. Slowly-cooled angrites (NWA 4590 and NWA 4801) have fractionated REE-patterns, chondritic to sub-chondritic  $^{187}\text{Os}/^{188}\text{Os}$  (0.1056–0.1195), as well as low-Re/Os (0.03–0.13), Pd/Os (0.071–0.946), and relatively low-Pt/Os (0.792–2.640). Sub-chondritic  $^{187}\text{Os}/^{188}\text{Os}$  compositions in NWA 4590 and NWA 4801 are unusual amongst planetary basalts, and their HSE and REE characteristics may be linked to melting of mantle sources that witnessed prior basaltic melt depletion. Angrite HSE–Yb systematics suggest that the HSE behaved moderately-incompatibly during angrite magma crystallization, implying the presence of metal in the crystallizing assemblage.

The new HSE abundance and  $^{187}\text{Os}/^{188}\text{Os}$  compositions indicate that the silicate mantle of the angrite parent body(ies) (APB) had HSE abundances in chondritic-relative proportions but at variable abundances at the time of angrite crystallization. The HSE systematics of angrites are consistent with protracted post-core formation accretion of materials with chondritic-relative abundances of HSE to the APB, and these accreted materials were rapidly, yet inefficiently, mixed into angrite magma source regions early in Solar System history.

© 2012 Elsevier B.V. All rights reserved.

### 1. Introduction

Angrites are broadly basaltic achondrite meteorites that crystallized from magmas generated within an early-formed differentiated parent body(ies), within  $\sim 2\text{--}10$  Myrs of the formation of calcium aluminum-rich inclusions (CAIs; e.g., Kleine et al., 2009; Markowski et al., 2007; Quitté et al., 2010). Absolute U–Pb chronology, coupled with relative-age chronometry from

\* Correspondence to: University of Alberta, Department of Earth and Atmospheric Sciences, 1-26 Earth Sciences Building, Edmonton, Alberta, Canada T6G 2E3. Tel.: +1 780 492 2676; fax: +1 780 492 2030.  
E-mail address: ariches@ualberta.ca (A.J.V. Riches).

$^{53}\text{Mn}\text{--}^{53}\text{Cr}$ ,  $^{26}\text{Al}\text{--}^{26}\text{Mg}$  and  $^{182}\text{Hf}\text{--}^{182}\text{W}$  systematics, show that angrites are some of the most ancient differentiated Solar System materials, with ages of 4564–4568 Ma (e.g., Amelin, 2008; Amelin et al., 2009; Baker et al., 2005; Connelly et al., 2008; Kleine et al., 2012; Lugmair and Galer, 1992; Nyquist et al., 2009). The relatively homogeneous  $\Delta^{17}\text{O}$  compositions ( $\Delta^{17}\text{O} = -0.072 \pm 0.007\%$  ( $1\sigma$ );  $\Delta^{17}\text{O}$  defined in the supplementary materials) that differ from terrestrial ( $\Delta^{17}\text{O} = 0\%$ ), lunar ( $0\%$ ), martian ( $\sim +0.3\%$ ), and howardite–eucrite–diogenite (HED;  $\Delta^{17}\text{O} = \sim -0.23\%$ ) compositions, indicate that angrites were derived from one or more distinct angrite parent bodies (APB), which experienced large-scale melting, differentiation, and O-isotopic homogenization (Clayton, 2003; Franchi, 2008; Greenwood et al., 2005; Mittlefehldt et al., 2008).

**Table 1**  
Highly-siderophile-element abundances (ppb) and osmium isotope data for angrite meteorites.

Sample	Group	Mass (g)	Os	Blk (%)	Ir	Blk (%)	Ru	Blk (%)	Pt	Blk (%)	Pd	Blk (%)	Re	Blk (%)	Re*	$\pm 2\sigma$	$^{187}\text{Re}/^{188}\text{Os}$	$\pm 2\sigma$	$^{187}\text{Re}^*/^{188}\text{Os}$	
Angra Dos Reis	Slowly-cooled	R <sup>a</sup>	0.191	0.0045	44.3	0.027	9	0.008	46	0.173	23	0.022	79	0.0014	99	0.0014	0.0007	1.49	1.08	1.475
		M	0.239	0.096	4.6	0.053	18	0.267	7	0.537	2	0.041	38	0.0148 <sup>b</sup>	95	0.0088	0.0005	0.74	0.95	0.440
D'Orbigny	Quenched	R	0.286	2.481	0.10	6.036	0.1	6.411	0.1	5.251	0.6	3.729	2	0.588	0.8	0.1558	0.0006	1.14	0.01	0.302
		M <sup>a</sup>	0.525	0.077	2.7	0.055	29	0.164	6	0.265	2	0.607	5	0.015	10	0.0168	0.0005	0.93	0.10	1.052
Sahara 99555	Quenched	R	0.265	0.240	1.06	0.249	2	0.547	1	0.937	4	0.420	4	0.050 <sup>c</sup>	10	0.0385	0.0006	1.01	0.10	0.776
		M <sup>a</sup>	0.896	0.121	1.02	0.137	21	0.203	3	0.458	0.6	0.504	3	0.025 <sup>b</sup>	4	0.0290	0.0003	1.01	0.04	1.164
A881371, 55	Quenched	M	0.194	0.307	0.37	0.288	2	0.315	12	0.801	4.4	0.239	46	0.039	10	0.0315	0.0003	0.61	0.10	0.496
NWA 1296	Quenched	M	0.304	0.0056	6.49	0.0088	13	0.0247	36	0.0110	67	0.0039	71	0.0008	64	0.0008	0.0001	0.66	0.64	0.718
NWA 4590	Slowly-cooled	R <sup>a</sup>	0.297	2.66	0.09	4.44	0.1	7.32	0.06	5.90	0.6	1.52	4	0.152	3	0.1577	0.0006	0.28	0.03	0.286
		M <sup>a</sup>	0.503	1.89	0.12	3.25	1	4.94	0.2	4.99	0.1	1.79	2	0.238 <sup>b</sup>	0.4	0.1157	0.0005	0.61	0.01	0.295
NWA 4801	Slowly-cooled	R <sup>a</sup>	0.314	14.16	0.005	15.0	0.03	28.4	0.01	12.4	0.3	1.68	3	0.379	0.5	0.349	0.002	0.128	0.007	0.119
		M <sup>a</sup>	0.448	10.47	0.024	10.07	0.4	9.20	0.1	8.28	0.1	0.74	5	0.279	0.4	0.297	0.004	0.128	0.006	0.136
NWA 4931	Anomalous	R	0.313	135	0.002	–	–	–	–	–	–	–	–	–	–	11.43	0.02	–	–	0.409
		M	0.310	114.9	0.003	133.36	0.03	216.04	0.01	243.55	0.004	173.40	0.03	9.08	0.02	9.99	0.02	0.381	0.005	0.419
		M	0.353	97.22	0.080	107.07	0.02	178.14	0.04	207.07	0.02	146.41	0.01	8.78	0.03	8.23	0.09	0.435	0.005	0.408
Sample		$^{187}\text{Os}/^{188}\text{Os}$	$\pm 2\sigma$	$^{187}\text{Os}/^{188}\text{Os}_i$	$\pm 2\sigma$	$\gamma\text{Os}_i$	$\pm 2\sigma$	Re/Os	Re*/Os	Pt/Os	Os/Ir	(Pt/Pd) <sub>N</sub>	(Pd/Os) <sub>N</sub>							
Angra Dos Reis	R*	0.2127	0.0062	0.095	0.121	–1.1	2.7	0.31	0.31	38.56	0.168	5.096	4.001							
	M	0.13094	0.00035	0.072	0.106	–24.8	1.3	0.15	0.09	5.583	1.819	8.621	0.342							
D'Orbigny	R	0.12007	0.00007	0.030	0.002	–68.9	2.0	0.24	0.06	2.117	0.411	0.924	1.212							
	M*	0.17927	0.00022	0.106	0.012	9.8	1.7	0.19	0.22	3.429	1.398	0.287	6.315							
Sahara 99555	R	0.15745	0.00020	0.077	0.012	–19.5	1.8	0.21	0.16	3.906	0.962	1.464	1.411							
	M*	0.18813	0.00013	0.109	0.005	13.0	1.8	0.21	0.24	3.792	0.882	0.596	3.363							
A881371, 55	M	0.13538	0.00019	0.087	0.011	–9.7	1.1	0.13	0.10	2.614	1.064	2.197	0.629							
NWA 1296	M	0.15287	0.00050	0.101	0.072	4.5	1.2	0.14	0.14	1.967	0.638	1.865	0.558							
NWA 4590	R*	0.11876	0.00006	0.097	0.003	0.8	0.5	0.06	0.06	2.222	0.598	2.553	0.460							
	M*	0.11947	0.00007	0.072	0.001	–25.6	1.1	0.13	0.06	2.640	0.582	1.830	0.763							
NWA 4801	R*	0.10556	0.00006	0.095	0.001	–0.8	0.2	0.03	0.02	0.873	0.945	4.825	0.096							
	M*	0.10696	0.00015	0.097	0.001	0.7	0.2	0.03	0.03	0.792	1.040	7.306	0.057							
NWA 4931	R	0.12852	0.00005	–	–	–	–	–	0.08	–	–	–	–							
	M	0.12927	0.00006	0.099	0.001	3.1	0.7	0.08	0.09	2.119	0.862	0.921	1.216							
	M	0.12839	0.00030	0.094	0.001	–2.3	0.8	0.09	0.08	2.130	0.908	0.928	1.214							

The uncertainty (%) associated with each abundance measurement reflects the propagated blank correction (Blk) derived from the measured blank of the corresponding analytical cohort. Uncertainties are highly variable and reflect the blank/sample ratio across the wide-range of observed HSE concentrations. The error associated with the reported  $^{187}\text{Re}/^{188}\text{Os}$  corresponds to the propagated uncertainty of the Re and Os abundances. Re\* is the concentration of Re calculated using the measured  $^{187}\text{Os}/^{188}\text{Os}$  isotope composition and the Os abundance of the sample, assuming a chondritic  $^{187}\text{Os}/^{188}\text{Os}$  at the time of sample formation (using Pb–Pb age data, supplementary materials), and  $^{187}\text{Re}^*/^{188}\text{Os}$  is calculated using this value. The uncertainty ( $2\sigma$ ) on the Re\* value represents the propagated uncertainties on the Os abundance and measured  $^{187}\text{Os}/^{188}\text{Os}$ . The Os-isotope composition of the sample at the time of formation is given by  $^{187}\text{Os}/^{188}\text{Os}_i$  (assuming the Pb–Pb ages shown in Table B15, supplementary materials).  $\gamma\text{Os}_i$  describes the difference between the  $^{187}\text{Os}/^{188}\text{Os}$  composition of the sample and the chondritic value at the time of formation, and is given by  $\gamma\text{Os}_i = 100 \times [(^{187}\text{Os}/^{188}\text{Os}_{\text{sample}(t)}) / (^{187}\text{Os}/^{188}\text{Os}_{\text{chondrite}(t)}) - 1]$ . R=reconnaissance measurement; M=main optimally spiked measurement. Sample aliquants in which ~20 to 50%, and > 60% of the total measured Re may represent recent additions of Re with radiogenic  $^{187}\text{Re}/^{188}\text{Os}$  compositions are denoted by (b) and (c), respectively. Aliquants considered to be least-contaminated by exogenous chondritic materials are denoted by (a). Highly-siderophile-element ratios normalized to the composition of Orgueil (after Horan et al., 2003) are denoted by (N), and the chondritic  $^{187}\text{Os}/^{188}\text{Os}$  composition follows Walker et al. (2002).

Given their early crystallization ages and O-isotopic homogenization, angrites might record information about silicate–metal equilibration during planetary differentiation on small early-formed planetesimals. A key suite of elements for examining planetary differentiation processes is the highly-siderophile elements (HSE; including Os, Ir, Ru, Rh, Pt, Pd, Re, and Au). Under low-pressure conditions applicable to small planets and asteroids, HSE have highly variable metal–silicate partition coefficients that are in excess of  $10^4$  (e.g., Borisov and Palme, 1997; Jones and Drake, 1986; Kimura et al., 1974; Mann et al., 2012; O'Neill et al., 1995). Consequently, the HSE might be expected to exhibit inter-element fractionation and occur at extremely low abundances in planetary mantles and their derivative rocks, such as angrites. Recent studies have shown that HSE occur in broadly chondritic-relative proportions in some angrites (Dale et al., 2012; Riches et al., 2010), and some authors argue that the APB contains HSE abundances broadly similar to those of Earth (Dale et al., 2012). The silicate mantles of the Earth, Moon, Mars, and the parent bodies of diogenites contain HSE in approximately chondritic-relative proportions and at higher abundances than predicted by low-pressure core formation; this has been interpreted as evidence supporting the addition of broadly chondritic materials during late accretion after the major-phases of core formation (e.g., Bottke et al., 2010; Brandon et al., 2000; 2012; Chou, 1978; Day et al., 2007; 2012a; Mitchell and Keays, 1981; Morgan and Lovering, 1967; Morgan et al., 1981; Ringwood, 1966; Walker et al., 2004). The comprehensive HSE abundance and Os-isotope study of angrites reported here provides complementary and new information to constrain the nature of post-core formation accretion to planetesimals in the early Solar System.

We analyzed eight texturally diverse angrite meteorites (Angra dos Reis; D'Orbigny; Asuka 881371; Sahara 99555; Northwest Africa [NWA] 1296; NWA 4801; NWA 4590; NWA 4931) to provide coupled HSE-abundances and  $^{187}\text{Re}$ – $^{187}\text{Os}$  systematics. We combine these data with new whole-rock trace-element abundances, as well as petrography and major-, trace- and HSE abundance data for minerals in the meteorites. Our objectives are to assess current petrogenetic models for angrites, and to evaluate conditions of metal–silicate equilibration and post-core formation accretion to the APB. These results provide new insight into the influence of oxygen fugacity and FeNi metal crystallization on HSE fractionation during angrite magma genesis, and this has important consequences for HSE abundances inferred for angrite magma source regions.

## 2. Sample preparation and analytical methods

All of the studied angrites are finds, except for Angra dos Reis, which was collected from the water of the Bay of Angra dos Reis (Brazil) 1 day after its observed fall. The angrite meteorite portions investigated here were obtained from several sources (supplementary materials). To avoid alteration or contamination from saw-blades, and/or other curatorial implements, we requested rock fractions from the interior portions of meteorites with minimal amounts of fusion crust and/or exterior surface material. Samples were examined using a binocular microscope to ensure against visible contamination or exterior adhering surface material, and surfaces were rinsed with ultra-pure water and dried prior to processing. Sample powders were prepared in a dust-free environment using an alumina mortar and pestle dedicated to processing angrites.

Osmium-isotope and HSE abundance data were obtained at the University of Maryland, using an analytical approach similar to a previous study of lunar crustal rocks (Day et al., 2010a). Initial reconnaissance (R) using approximately 0.19–0.31 g of powder was conducted on the first set of prepared powder fractions for

Angra dos Reis, D'Orbigny, Sahara 99555, NWA 4801, NWA 4590, and NWA 4931. Subsequently, 0.24–0.90 g sample splits of these meteorites were crushed and optimally spiked with guidance from the small-aliquant analyses. These analyses are referred to as main fractions, or 'M', for the remainder of this paper. For two of the samples (Asuka 881371 and NWA 1296), the limited available sample mass precluded multiple Os-isotope and HSE abundance determinations, and for this reason, guidance for optimal spiking was obtained from compositional similarities with D'Orbigny and Sahara 99555 (e.g., Floss et al., 2003; Jambon et al., 2005). Although we expected the HSE abundances of angrites to be broadly similar to, or lower than, those of lunar mare basalts ( $< 0.001$ – $0.038$  ppb Os; Day et al., 2007) because of their derivation from a highly-differentiated parent body(ies) (e.g., Greenwood et al., 2005), our initial investigation showed that HSE concentrations of angrites range from  $\sim 0.005$  ppb up to 135 ppb Os (Table 1). For this reason, the reconnaissance analysis of one sample (NWA 4931) was under-spiked, and only Os abundance and  $^{187}\text{Os}/^{188}\text{Os}$  data are presented for this aliquant. For completeness, the data for the remainder of the samples, for both reconnaissance and replicate aliquants, are reported in Table 1, allowing estimation of the degree of local HSE heterogeneity within samples. However, it should be noted that, in some cases, uncertainties of HSE concentrations for small aliquants (190–240 mg) approach 100%.

Osmium-isotope compositions were determined in negative-ion mode using a *ThermoFisher Triton* thermal ionization mass-spectrometer at the University of Maryland. External precision of  $^{187}\text{Os}/^{188}\text{Os}$  during the analytical campaign was better than  $\pm 0.2\%$  ( $^{187}\text{Os}/^{188}\text{Os} = 0.11380 \pm 20$ ,  $n = 13$ ;  $2\sigma_{\text{stddev}}$ ), and was determined on 3.5–35 pg loads of the UMCP Johnson–Matthey standard reference solution. Iridium, Pt, Pd, Ru, and Re abundances were measured using a *Cetac Aridus* desolvating nebulizer coupled to a *ThermoFisher Element 2* inductively coupled plasma mass-spectrometer (ICP-MS) operated in low-resolution mode. External reproducibility ( $2\sigma$ ) on  $> 10$  standard analyses for each analytical session was better than 0.2% for 0.01–1 ppb solutions of Re and Pt, and better than 0.4% for Ir, Ru, and Pd. External reproducibility of measurements was also monitored by regular analysis of reference materials (GP13 peridotite standard), yielding reproducibilities of 4.3–16% for HSE abundances and 0.6% for  $^{187}\text{Os}/^{188}\text{Os}$  ( $2\sigma$ ,  $n = 9$ ; Day et al., 2012a).

Total procedural blanks (TPB;  $n = 5$ ) had  $^{187}\text{Os}/^{188}\text{Os}$  averaging  $0.162 \pm 0.041$ , and quantities (in picograms) of  $0.4 \pm 0.4$  [Os],  $1.8 \pm 1.7$  [Ir],  $5.0 \pm 2.5$  [Ru],  $6.7 \pm 2.7$  [Pt],  $16.2 \pm 14.8$  [Pd], and  $0.8 \pm 0.4$  [Re]. All concentrations and isotopic compositions were corrected for the blank obtained for the corresponding sample cohort. The relative uncertainty associated with blank contributions of Re is large, and for this reason,  $\text{Re}^*$  values are also reported in Table 1. This value is the concentration of Re calculated by assuming chondritic  $^{187}\text{Os}/^{188}\text{Os}$  at the estimated time of sample crystallization using the measured Os concentrations, and measured  $^{187}\text{Os}/^{188}\text{Os}$  compositions, to calculate  $\text{Re}^*/\text{Os}$ .

Whole-rock trace-element abundance analyses were performed at the University of Maryland using methods outlined in Day et al. (2012b), with external reproducibility and accuracy for all measured trace-element abundances (except HSE) being better than  $\pm 5\%$  ( $2\sigma$ ; supplementary materials). Whole-rock major-element analyses were performed at the University of Tennessee, using methods outlined in Riches et al. (2011). Mineral major-element analyses were performed at the University of Tennessee using a *Cameca SX-100* electron microprobe, and *in situ* laser-ablation ICP-MS analysis of silicates and metals were performed at the University of Notre Dame and the University of Maryland, respectively, using *New Wave 213 nm* laser-ablation systems coupled to *Element 2* ICP-MS instruments. Further details of

**Table 2**  
Angrite bulk-rock trace-element abundance data reported in ppm.

	AdoR	S 99555	D'Orbigny	D'Orbigny	A 881371	NWA 1296	NWA4590	NWA4801	NWA4801	NWA4931
Mass (mg)	50.5	46.1	50.5	65.8	50.3	63.3	50.3	50.1	50.8	50.8
Li	1.84(3)	6.17(3)	5.8(1)	6.36	6.15(3)	6.87	11.2(3)	4.66(2)	4.07(4)	3.1(1)
Sc	48.8(3)	46.9(2)	42.4(6)	47.3	35.6(4)	49.9	41.4(4)	48(1)	42(2)	17.0(4)
V	182.3(8)	132(2)	122(3)	130.2	103(1)	137.0	101.1(2)	139(4)	122(7)	67(2)
Cr	1519(5)	291(9)	273(8)	282	928(1)	488	364(5)	1470(48)	1361(87)	1885(66)
Co	17.17(6)	32.9(7)	31.5(9)	33.8	47.7(4)	29.4	24.93(6)	20.0(4)	17.4(8)	240(5)
Ni	129(8)	86(1)	73.9(1)	66.6	103(3)	57.3	91(2)	98(1)	86(2)	2618 ± 107
Cu	26.67(2)	12.7(5)	12.2(3)	11.26	4.2(2)	9.44	11.1(1)	15.7(6)	13.9(9)	7.73(7)
Rb	0.02(2)	0.85(5)	0.41(3)	0.434	0.110(7)	0.107	0.315(7)	0.07(2)	0.04(1)	0.048(3)
Sr	123(4)	93.91(6)	96(1)	110.0	79.54(5)	101.0	133(1)	108.6(6)	100(3)	63.9(1)
Y	54.6(6)	19.6(3)	19.8(2)	20.40	14.6(3)	21.59	30.9(2)	31.6(4)	27(1)	7.04(5)
Zr	150.8(5)	57.3(2)	57.7(6)	59.2	45(2)	58.8	81.4(2)	104(1)	91(4)	21.47(8)
Nb	7.3(9)	3.64(4)	3.74(5)	3.7	2.6(1)	3.8	1.471(3)	3.11(5)	2.7(1)	0.21(1)
Mo	0.0905(8)	0.209(4)	0.18(1)	0.261	0.270(9)	0.382	0.14(2)	0.074(5)	0.050(4)	0.612(4)
Cs	0.0003(2)	0.161(2)	0.0214(4)	0.0231	0.0040(2)	0.0023	0.01972(1)	0.003(2)	0.0024(2)	0.00273(4)
Ba	20.9(3)	37.27(3)	50.01(2)	49.35	23(1)	40.78	81(2)	40.5(6)	36.2(8)	72.5(2)
La	6.2(2)	3.536(5)	3.753(2)	3.425	2.50(6)	3.333	3.19(4)	3.43(1)	2.96(7)	0.522(3)
Ce	18.5(3)	9.01(2)	9.22(4)	8.943	6.3(1)	9.097	8.8(1)	10.68(6)	9.3(1)	1.72(1)
Pr	3.09(4)	1.285(4)	1.331(9)	1.301	0.99(3)	1.295	1.35(1)	1.75(1)	1.52(3)	0.299(6)
Nd	17.2(3)	6.70(5)	6.92(1)	6.953	4.9(1)	7.079	7.42(9)	10.0(1)	8.6(2)	1.89(1)
Sm	5.9(1)	2.127(4)	2.15(2)	2.169	1.58(6)	2.222	2.61(5)	3.46(3)	3.02(8)	0.69(1)
Eu	1.81(7)	0.821(8)	0.840(7)	0.858	0.63(2)	0.845	1.06(3)	1.152(8)	1.03(1)	0.39(1)
Gd	7.3(2)	2.70(5)	2.718(4)	2.756	2.09(4)	2.880	3.51(7)	4.43(4)	3.85(5)	0.93(2)
Tb	1.39(5)	0.505(6)	0.508(2)	0.499	0.38(1)	0.527	0.70(2)	0.844(5)	0.733(9)	0.183(4)
Dy	9.2(3)	3.40(3)	3.384(9)	3.479	2.60(8)	3.685	4.9(1)	5.60(5)	4.90(5)	1.26(3)
Ho	2.03(8)	0.76(1)	0.760(4)	0.752	0.57(2)	0.801	1.14(2)	1.22(1)	1.08(1)	0.284(7)
Er	5.6(2)	2.16(2)	2.15(1)	2.178	1.66(6)	2.317	3.32(7)	3.388(7)	2.95(1)	0.82(2)
Tm	0.83(3)	0.332(2)	0.3328(3)	0.321	0.243(9)	0.344	0.52(1)	0.507(1)	0.4422(4)	0.132(2)
Yb	5.0(1)	2.11(1)	2.09(2)	2.120	1.60(6)	2.230	3.31(7)	3.106(1)	2.72(7)	0.88(3)
Lu	0.72(1)	0.322(2)	0.31560(1)	0.307	0.24(1)	0.325	0.50(1)	0.460(2)	0.404(6)	0.141(3)
Hf	2.70(7)	1.63(2)	1.58(2)	1.552	1.24(9)	1.593	2.20(5)	2.564(8)	2.24(3)	0.72(2)
Ta	0.470(9)	0.206(4)	0.206(3)	0.190	0.148(9)	0.194	0.128(3)	0.235(4)	0.203(8)	0.027(3)
W	0.19(7)	0.35(5)	0.27(4)	0.216	0.23(3)	0.263	0.31(4)	0.97(7)	0.82(3)	0.13(3)
Pb	3.1(2)	0.45(3)	1.37(2)	1.352	0.16(1)	0.294	0.38(3)	0.30(1)	0.258(4)	0.2(2)
Th	0.74(5)	0.50(2)	0.454(9)	0.451	0.33(2)	0.451	0.325(9)	0.283(4)	0.242(2)	0.028(2)
U	0.20(1)	0.106(3)	0.082(1)	0.077	0.082(5)	0.067	0.096(4)	0.094(1)	0.081(1)	0.032(2)

AdoR=Angra dos Reis, S 99555 = Sahara 99555, and A 881371=Asuka 881371. Uncertainties ( $2\sigma_{\text{stdev}}$ ) associated with measured trace-element concentrations are reported in parentheses and correspond to the least decimal or significant figure cited.

methods used to prepare samples and obtain bulk-rock Re-Os isotope and HSE abundance data, major- and trace-element concentrations, and *in situ* mineral-chemical data are reported in the supplementary materials.

### 3. Results

#### 3.1. Petrographic and mineralogical characteristics

Angrites are texturally diverse achondritic meteorites (Table 1), with variable grain sizes that are typically 0.2–3 mm in maximum dimension, corresponding to older quenched-, and younger slowly-cooled angrites, respectively. Phase assemblages and mineral compositional ranges reported in this study are broadly consistent with previous observations (e.g., Floss et al., 2003; Jambon et al., 2005, 2008; Keil, in press; Mittlefehldt and Lindstrom, 1990; Mittlefehldt et al., 2002; supplementary materials). Notably, some angrites contain FeNi metal grains accounting for as much as 6 modal % (kamacite+tetrataenite in NWA 4801, and kamacite in NWA 4931).

Major- and trace-element abundances determined for constituent minerals of angrites are reported in the supplementary materials. Abundances of the HSE were measured in mineral grains from NWA 4931 (supplementary materials), and co-existing silicate phases contain no detectable HSE concentrations. Hercynitic spinel is associated with appreciable quantities of Pt (0.89 ppm) and Pd (2.22 ppm). Metals in NWA 4931 contain total

HSE abundances exceeding 50 ppm, which are in broadly chondritic-relative proportions (supplementary materials), and the HSE in these kamacite grains account for the majority of the bulk-rock HSE budget of this meteorite. A reconstructed bulk-rock HSE composition, calculated by combining modal abundances (supplementary materials) and representative mineral HSE abundances, has broadly chondritic-relative abundances of the HSE, but at lower concentrations than measured in bulk-rock fractions. These differences probably reflect variations in the modal proportions of metal determined during petrographic study versus those of sample powders.

#### 3.2. Whole-rock trace-element abundances of angrites

New bulk-rock trace-element abundance data are reported in Table 2 and plotted in Fig. 1. The relative and absolute abundances of whole-rock rare-earth-elements (REE) in the studied angrites define three different relative abundance patterns: (1) Angra dos Reis, NWA 4801, and NWA 4590 have elevated middle-REE (MREE) relative to light-REE (LREE); ( $[\text{La}/\text{Sm}]_{\text{N}}=0.61\text{--}0.77$ ), and heavy-REE (HREE) are low to moderately elevated relative to MREE ( $[\text{Sm}/\text{Yb}]_{\text{N}}=1.23\text{--}1.29$  in Angra dos Reis and NWA 4801, and  $[\text{Sm}/\text{Yb}]_{\text{N}}=0.87$  in NWA 4590). Angra dos Reis and NWA 4801 have negative Eu-anomalies ( $[\text{Eu}/\text{Eu}^*]=0.84$  and  $0.89\text{--}0.91$ , respectively), and NWA 4590 is characterized by a slight positive Eu-anomaly (1.06); (2) the quenched-angrite group (NWA 1296, Sahara 99555, D'Orbigny, Asuka 881371) define broadly flat chondrite relative REE-patterns ( $[\text{La}/\text{Yb}]_{\text{N}}=1.08\text{--}1.24$ ) at  $10\text{--}15 \times \text{CI}$ -chondrite; and

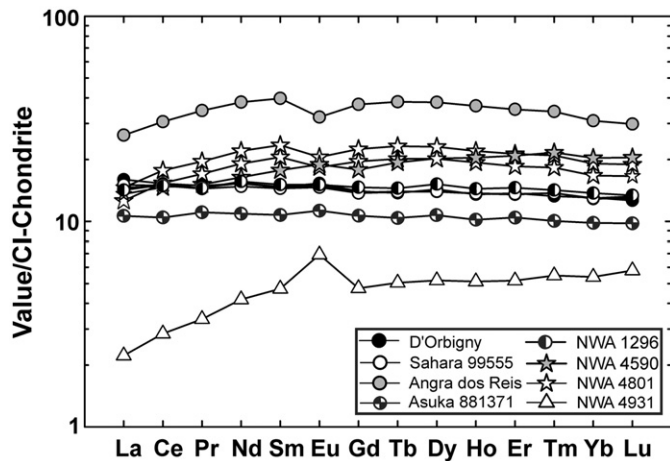


Fig. 1. Whole-rock REE concentrations of angrite bulk powder fractions normalized to the CI-chondrite estimate of Anders and Grevesse (1989).

(3) NWA 4931 has the lowest absolute abundances of REE, with the lowest  $(\text{La}/\text{Yb})_N$  (0.41), and a positive Eu-anomaly ( $[\text{Eu}/\text{Eu}^*]_N = 1.46$ ). A striking aspect of the new trace-element abundance data is the generally lower trace-element concentrations in NWA 4931 compared with other angrites (e.g., REE concentrations  $< 10 \times$  CI-chondrite in NWA 4931). The major exceptions are high Ba (72.5 ppm), Co, and Ni contents (240 and 2620 ppm, respectively) in NWA 4931; Ni and Co concentrations in this meteorite are an order of magnitude higher than in other angrites.

### 3.3. Highly-siderophile-element abundances and osmium-isotope compositions of angrites

Angrite meteorites span a considerable range of HSE abundances from samples with low-HSE contents ( $< 0.005$  ppb Os; NWA 1296; Angra dos Reis) to samples that have HSE concentrations  $\sim 0.3 \times$  CI-chondrite (97.2–135 ppb Os; NWA 4931; Fig. 2). The  $^{187}\text{Os}/^{188}\text{Os}$  of the studied angrites range from 0.1056 to 0.213, with measured  $^{187}\text{Re}/^{188}\text{Os}$  ranging from 0.128 to 1.49 (Table 1), and this range of Re–Os isotope compositions extends beyond external analytical precision (section 2). Comparison of individual aliquants shows that intra-sample HSE abundances and  $^{187}\text{Os}/^{188}\text{Os}$  vary beyond analytical uncertainties in some angrites. For this reason, where replicate measurements of individual angrites were possible we illustrate the percentage of intra-sample HSE abundance and Os-isotope variation by calculating the relative standard deviation [RSD] for two to three aliquants. The coarse-grained, slowly-cooled angrites have more reproducible HSE abundances and  $^{187}\text{Os}/^{188}\text{Os}$  (generally 12–55% and 0.42–0.93% relative standard deviation [RSD] for HSE abundances and Os-isotope compositions in NWA 4590 and NWA 4801, respectively) than quenched-angrites. Ruthenium abundances in NWA 4801 show the greatest degree of variation (72% [RSD]). In contrast, quenched-angrites (D'Orbigny and Sahara 99555), and Angra dos Reis show significant variations in HSE abundances and  $^{187}\text{Os}/^{188}\text{Os}$  between powders prepared from different portions of these meteorites (13–139% [RSD] and 13–34% [RSD] for HSE abundances and  $^{187}\text{Os}/^{188}\text{Os}$ , respectively). Quenched-angrites, NWA 1296, and a portion of Angra dos Reis have the lowest total HSE abundances ( $\Sigma\text{HSE}=0.24\text{--}0.5$  ppb), and NWA 4931 has the highest total HSE concentrations ( $\Sigma\text{HSE}=890$  ppb) and an HSE abundance pattern with chondritic-relative abundances (Fig. 2). The most reproducible HSE abundances and Os-isotope compositions were obtained from NWA 4931 (2–16% and 0.37% [RSD], respectively).

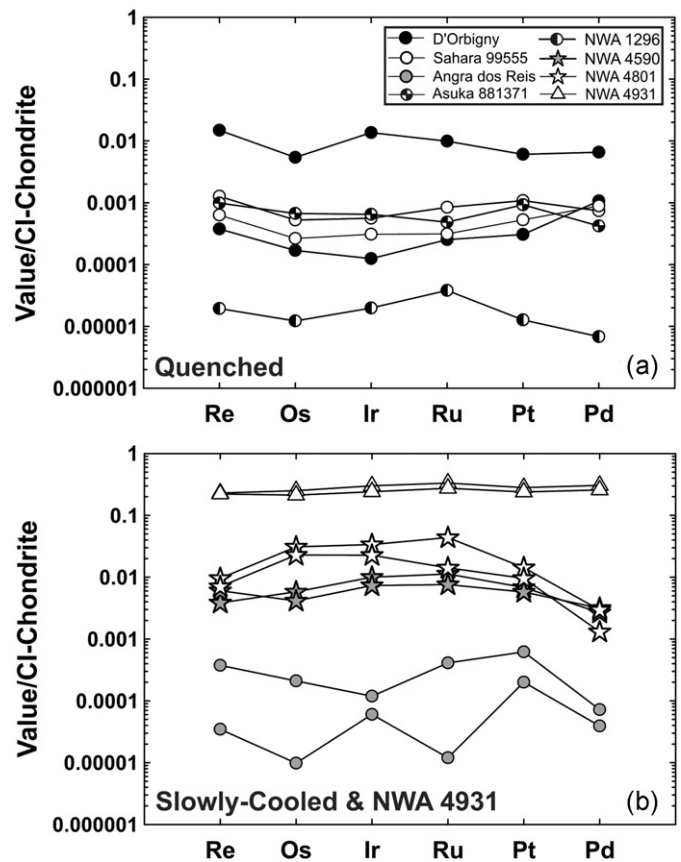


Fig. 2. Highly-siderophile-element (HSE) abundances of bulk-rock fractions of (a) quenched-angrites, and (b) slowly-cooled angrites and texturally anomalous NWA 4931 normalized to the composition of Orgueil (Horan et al., 2003). Elements are plotted in order of increasing volatility under reducing conditions from left to right.

The Re–Os isotope compositions of four angrite powder aliquants, including portions of D'Orbigny, Sahara 99555, and NWA 4590, do not plot within analytical uncertainties of the 4.563 Ga reference line (Fig. 3(a)). However, propagated uncertainties (including external precisions and blank contributions) are strongly dependent on Re abundances and  $^{187}\text{Re}/^{188}\text{Os}$ , and the uncertainties associated with these measurements. Ten other angrite aliquants coincide with, or fall close to, a 4.563 Ga reference line (Fig. 3(a) and (b)), which represents single-stage evolution of variably fractionated materials from a uniform chondritic reservoir at a time broadly coincident with angrite crystallization.

## 4. Discussion

### 4.1. Alteration and post-crystallization Re–Os isotope disturbance

Although some angrite portions yield Re–Os isotope compositions that coincide with the 4.563 Ga reference line (Fig. 3), there is dispersion of individual angrite samples about this line. The majority of angrites have measured Re concentrations that differ, beyond analytical uncertainties, from calculated  $\text{Re}^*$  abundances (Table 1). These characteristics are consistent with varying amounts of disturbance of Re and/or Os, long after initial angrite magma crystallization. Previous studies of chondritic materials, achondritic meteorites, and returned (Apollo) lunar samples have reported similar Re–Os disturbance attributed to either: (1)

low-temperature alteration in terrestrial environments that potentially adds or removes Re and/or Os (e.g., Brandon et al., 2012; Day et al., 2012b; Horan et al., 2009); (2) surface exposure and neutron capture by W leading to neutron-fluence effects on Re (c.f., Day et al., 2010a; Herr et al., 1971; Michel et al., 1972); or (3) contamination by terrestrial materials during sample preparation (Day et al., 2010a).

With the exception of the observed fall of Angra dos Reis, all other studied angrites are finds, and were subjected to varying degrees of low-temperature alteration in terrestrial environments (deserts) for significant periods of time. For these reasons, the most probable origins of Re–Os isotope disturbance in angrite meteorites are from relatively recent (< 1 Ma) low-temperature alteration on Earth.

The precise nature of low-temperature alteration experienced by angrites is not known in detail, but analogies can be drawn from comparable petrographic, chemical, and isotopic alteration signatures reported for other achondrites. NWA 4931 contains altered metals broadly comparable to altered metals and sulfides reported in a recent investigation of brachinites (Day et al., 2012b). The oxidative low-temperature alteration of brachinite metals and sulfides has been linked to mobilization of Re within these meteorites, with other HSE showing only limited evidence of disturbance. Mobilization of Re will generate dispersion on a  $^{187}\text{Re}/^{188}\text{Os}$ – $^{187}\text{Os}/^{188}\text{Os}$  plot, with removal of Re leading to lower Re/Os than predicted from the time-integrated in-growth of  $^{187}\text{Os}$  (plot to the left of the 4.563 Ga reference line), and addition of Re leading to higher Re/Os (plot to the right of the 4.563 Ga reference line). It is also possible that Re–Os disturbance occurred through physical exchange with terrestrial materials (e.g., during exposure to near-surface fluids). Rhenium is sensitive to terrestrial desert alteration, as relatively high-abundances of Re are commonly present in continental environments (e.g., estimates for upper continental crust are  $\sim 0.2$  ppb Re with  $^{187}\text{Re}/^{188}\text{Os}=34.5$ ; Peucker-Ehrenbrink and Jahn, 2001). This contrasts with Os that generally occurs in much lower concentrations in continental environments (estimates for average upper continental crust are  $< 0.05$  ppb Os; Peucker-Ehrenbrink and Jahn, 2001).

Some of the Re–Os isotopic deviations observed in angrites preclude use of the Re–Os isotope system for a precise age determination. However, the degree of open-system behavior appears to be minor to negligible for the other HSE (Os, Ir, Ru, Pt, Pd). This is indicated by the limited variations in the inter-element ratios of these other HSE (supplementary materials). Thus, whereas angrite Re abundances and  $^{187}\text{Re}/^{188}\text{Os}$  compositions are highly sensitive to terrestrial alteration in meteorites, we argue that the relative and absolute abundances of the other HSE and the measured  $^{187}\text{Os}/^{188}\text{Os}$  in angrites remain high-fidelity recorders of processes acting on the APB.

#### 4.2. Impactor contamination and involvement of felsic crust in NWA 4931

During residence at or close to the APB surface, and through impact-ejection, angrites may have been subject to HSE-rich impactor contamination that post-dated magmatic crystallization. Such contamination is a localized near-surface modification process, and differs from late accretion following core formation, which requires addition of HSE to magma source regions prior to the extraction and crystallization of angrite parental melts. Impact contamination processes on the APB are analogous to those common among lunar rocks, where some crustal rocks (formerly treated as “pristine” samples) show evidence for HSE enrichment, tending toward chondritic-relative abundances of the HSE (e.g., Day et al., 2010a).

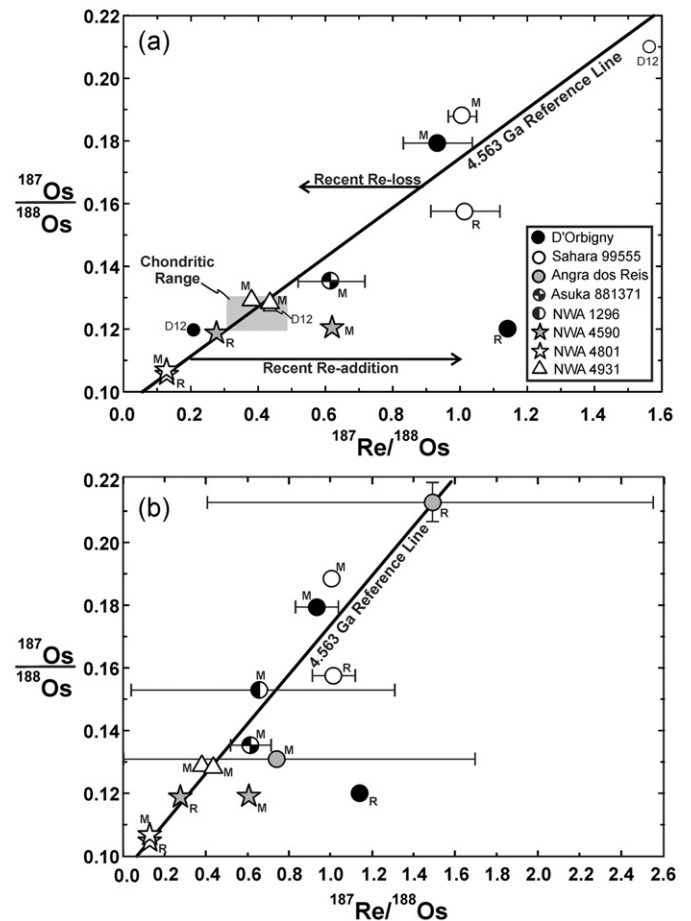


**Fig. 3.** Rhenium–Os isotope compositions of angrites determined by isotope dilution showing the main optimally spiked aliquant (M) and reconnaissance (R) aliquant of each studied sample. Uncertainties ( $2\sigma$ ) are less than symbol size unless shown otherwise. Two fractions of Angra dos Reis and an aliquant of NWA 1296 (b) with low-HSE abundances are omitted from (a) as the uncertainties on the measured values extend beyond the figure area. The 4.563 Ga reference line represents single-stage Re–Os isotope evolution from a chondritic  $^{187}\text{Os}/^{188}\text{Os}$  reservoir and is calculated assuming a Solar System initial of  $^{187}\text{Os}/^{188}\text{Os} = 0.9524 \pm 0.0011$  and a  $^{187}\text{Re}$ -decay constant of  $1.666 \times 10^{-11}$  (Smoliar et al., 1996). The range of Re–Os isotope compositions determined for chondritic meteorites (after Fischer-Gödde et al., 2010; Horan et al., 2003; van Acken et al., 2011; Walker et al., 2002) are shown as a solid gray box in (a). Deviations of measured Re–Os isotope compositions from the 4.563 Ga reference line that result from recent Re disturbance are illustrated by black arrows. Data points labelled D12 correspond to those reported by Dale et al. (2012).

The most likely contender for an angritic impact-melt rock is NWA 4931. This meteorite has a poikilitic texture (supplementary materials), the highest bulk-rock HSE content of any studied angrite, chondritic-relative abundances of the HSE, and chondritic  $^{187}\text{Os}/^{188}\text{Os}$ . Furthermore, NWA 4931 is paired with NWA 2999, and *in situ* LA-ICP-MS studies of this meteorite have indicated the presence of chondritic metals that may be of impact origin (Humayun et al., 2007; supplementary materials). Bulk-mixing models suggest that the HSE-abundances and Os-isotope composition of NWA 4931 may be accounted for by the presence of  $\sim 30$  wt.% of chondritic materials (Fig. 4; supplementary materials), but addition of chondritic metals alone (through impact-driven accretion and vaporization) requires substantially less mass to account for the observed HSE characteristics.

In addition to elevated HSE abundances, NWA 4931 is characterized by a positive Eu-anomaly and lower absolute REE abundances than other angrites. These characteristics differ considerably from the two other identified REE-groups and suggest an origin for NWA 4931

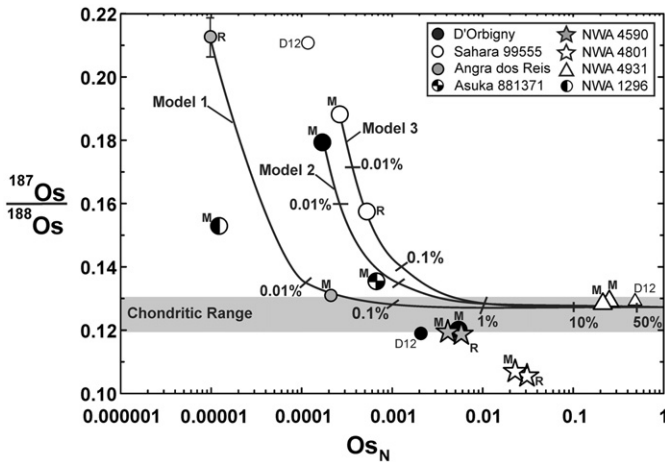


**Fig. 4.** Osmium-isotope compositions and Os abundances normalized to the composition of Orgueil (Horan et al., 2003) of angrites. Measured angrite compositions are compared to models of simple mixing between chondritic materials and (1) the reconnaissance aliquant (R) of Angra dos Reis (Model 1), (2) the main optimally-spiked aliquant (M) of D'Orbigny (Model 2), and (3) the M-aliquant of Sahara 99555 (Model 3). The range of  $^{187}\text{Os}/^{188}\text{Os}$  isotope compositions determined for chondritic meteorites (after Fischer-Gödde et al., 2010; Horan et al., 2003; van Acken et al., 2011; Walker et al., 2002) is shown as a gray bar. Data points labelled D12 correspond to those reported by Dale et al. (2012).

from a plagioclase-rich protolith. Mass-balance calculations, to remove  $\sim 30\%$  chondritic impactor in order to estimate initial protolith composition ( $[\text{REE}]_N=2.8$ ;  $[\text{Eu}]_N=4.5$ ), suggest that the impacted lithology does not match the extremely low-REE abundances and the large-positive Eu-anomalies of pristine lunar anorthosites (e.g., Wakita and Schmitt, 1970), or the more LREE-enriched character of felsic asteroidal crust (e.g., GRA 06128/9 meteorites; Day et al., 2009). Instead, the composition of NWA 4931 more closely matches a plagioclase-rich 'basaltic' composition, and hints at the possibility that the APB may have an early-formed heterogeneous

crust composed of both broadly basaltic and more felsic lithologies (Fig. 5). Because the HSE contents of NWA 4931 are dominated by impact additions in near-surface environments, this sample is excluded from subsequent discussion sections exploring the parent body processing and internal APB HSE characteristics.

#### 4.3. Addition of exogenous chondritic material to quenched-angrites

With the exception of NWA 4931, the studied angrites exhibit chondrite-normalized HSE-patterns that range from relatively flat (e.g., Asuka 881371; Sahara 99555) to moderately fractionated (e.g., NWA 4801), with Os abundances ranging between 0.0045 and 14.2 ppb. Intra-sample variations in HSE abundances and Os-isotope compositions have been reported for terrestrial samples, and these differences are often attributed to modal variations in small sample fractions. However, this hypothesis does not provide a unique explanation for the angrite HSE characteristics. The most straight-forward explanation for the variations in absolute HSE abundances between different aliquants of D'Orbigny, Sahara 99555, Asuka 881371, NWA 1296, and Angra dos Reis are from minor additions of exogenous chondritic materials during or subsequent to magmatic crystallization. In this model, 'pristine' angrite-magmas contain low HSE abundances ( $\Sigma\text{HSE} \leq 0.24\text{--}2.44$  ppb), which are highly sensitive to contamination by exogenous chondritic materials. Thus, HSE abundance variations in quenched-angrites may reflect small amounts of assimilation of regolith containing chondritic materials rich in HSE; these assimilated materials were incompletely homogenized by rapidly cooled angrite lavas or shallow-level intrusive bodies. Alternatively, exogenous chondritic HSE may have been added to quenched-angrites as minor impact additions in near-surface environments. The first of these scenarios is preferred as there is little petrographic evidence for impact disturbance in quenched-angrites. To quantitatively evaluate potential exogenous HSE additions to angrites, mixing curves were calculated between a chondritic impactor and three possible protoliths, represented by the

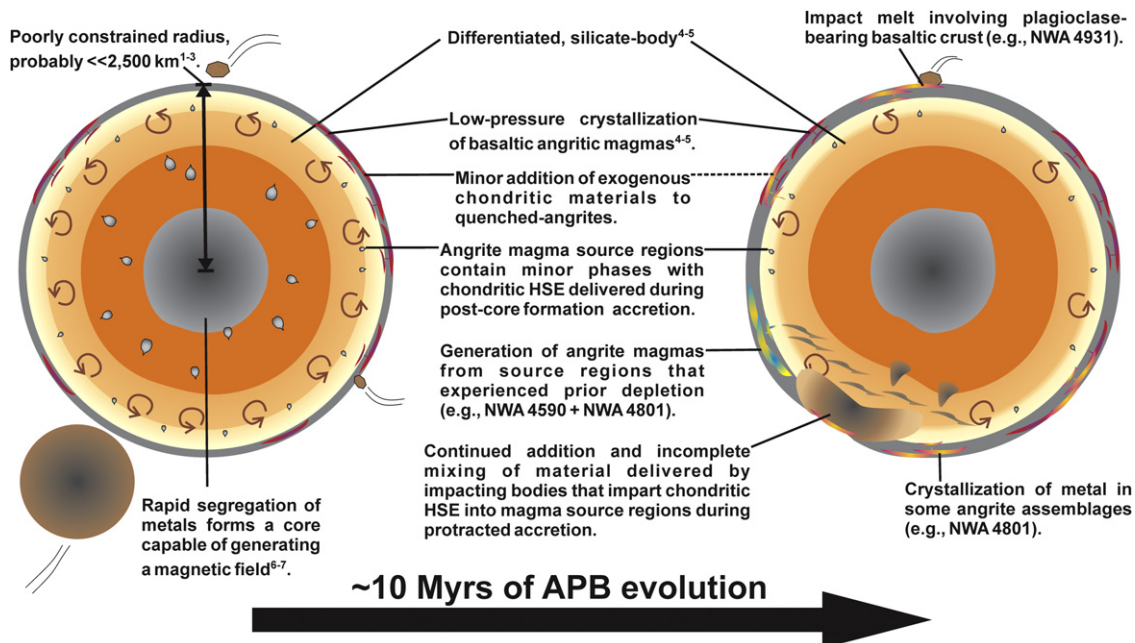


**Fig. 5.** Schematic illustration of early core formation, generation of angrite magmas, and addition of impact material on the angrite parent body(ies) (APB) shown here as a single planetary pre-cursor. The decay of short-lived radionuclides such as  $\text{Al}^{26}$  + energy imparted during collisions supplies heat capable of generating a magma ocean, and heterogeneous (silicate) source regions may have formed during magma ocean crystallization (after Greenwood et al., 2005). Impact contributions may have involved bodies of broadly chondritic compositions with widely varying sizes, and inefficient mixing of these materials in early-formed bodies cautions against assumptions of homogenous HSE abundances at all parent body scales. <sup>1</sup>Rivkin et al., 2007; <sup>2</sup>Trilling et al., 2007; <sup>3</sup>Scott and Bottke, 2011; <sup>4</sup>Mittlefehldt and Lindstrom, 1990; <sup>5</sup>Floss et al., 2003; <sup>6</sup>Markowski et al., 2007; <sup>7</sup>Weiss et al. (2008).

reconnaissance (R) aliquant of Angra dos Reis and the main (M) aliquant of Sahara 99555 and D'Orbigny. With this calculation between <0.01 and 0.8% exogenous chondritic material is required to explain the HSE abundance and Os-isotope compositions of the M-aliquant of Angra dos Reis, and the R-aliquant of D'Orbigny and Sahara 99555 (Fig. 4; supplementary materials). If it is assumed that the R-aliquant of Angra dos Reis is similar to a pristine pre-cursor of NWA 1296, then less than 0.01% exogenous chondritic addition would be required to explain the HSE abundances in NWA 1296. Similarly, Asuka 881371 may result from the addition of <0.1% chondritic material to a 'pristine' magmatic protolith similar to the M-aliquant of D'Orbigny. Samples that do not conform to impactor contamination include NWA 4801 and NWA 4590, both of which have sub-chondritic  $^{187}\text{Os}/^{188}\text{Os}$  and fractionated REE-patterns.

#### 4.4. Igneous processes on the angrite parent body

Several petrogenetic models have been proposed to explain the formation of angrites. Kurat et al. (2004) and Varela et al. (2003, 2005) provided detailed mineralogical observations and major- and trace-element compositions of the D'Orbigny meteorite and its constituent glasses. These authors argued that D'Orbigny was generated through multi-stage 'non-igneous' nebular processes, broadly analogous to those that may have generated CAIs. Some angrites contain HSE that are fractionated with respect to chondrites, and the relative abundances of HSE are not consistent with volatility controlled processes alone, as would be indicated by depletions or enrichments in the more volatile HSE Pd (or Au). Thus, the absolute and relative abundances of the HSE in D'Orbigny are not compatible with a direct nebular origin for angrites.

As discussed above (Section 4.3), several aliquants of the quenched-angrites, and slowly-cooled Angra dos Reis show significant intra-sample variations in HSE abundances and  $^{187}\text{Os}/^{188}\text{Os}$  compositions, consistent with the addition of exogenous chondritic material imparted in near-surface environments (Fig. 4). For these reasons, the HSE compositions of these angrites do not solely reflect the HSE characteristics of magma source regions in the APB interior. The following discussion of igneous processes is focused on the HSE characteristics of the least-contaminated angrite aliquants (Table 1).

The HSE are particularly valuable tracers for understanding the origin of angrites, because early-formed and undifferentiated materials (e.g., chondrites, CAIs) are characterized by elevated abundances of these elements (e.g., Anders and Grevesse, 1989; Crocket et al., 1967; Horan et al., 2003; Kallemeyn and Wasson, 1981; van Acken et al., 2011). During magmatic differentiation of a broadly chondritic pre-cursor, HSE are depleted in silicate reservoirs by: (1) silicate-metal equilibration, whereby the resultant silicate mantle would be effectively stripped of the HSE (e.g., Borisov and Palme, 1997; Jones and Drake, 1986; Kimura et al., 1974; O'Neill et al., 1995); and/or (2) Fe-Ni-sulfide and silicate-melt extraction (e.g., Day et al., 2012b; Jones et al., 2003; Rehkämper et al., 1999). Therefore, the observations that some angrites are depleted in the HSE by as much as a factor of one hundred relative to CI-chondrite, and that some angrites also have fractionated relative-abundances of HSE strongly implies that angrites have witnessed partial to extensive metal-silicate equilibration associated with core formation on the APB, and are products of magmatic differentiation.

A striking aspect of the new HSE abundance data for angrites is the fractionated chondrite-normalized HSE-patterns for NWA 4801, and to a lesser extent NWA 4590 (Fig. 2). These angrites are characterized by more reproducible, yet distinct, and more fractionated HSE-patterns compared to other angrites. Further,

the R- and M-aliquants of both samples yield  $^{187}\text{Os}/^{188}\text{Os}$  that are considerably lower than are typical of bulk chondrites (Fischer-Gödde et al., 2010; Horan et al., 2003; Walker et al., 2002), and these values are among the lowest Os-isotope ratios measured in bulk planetary materials, with only some non-metallic components of ordinary chondrites characterized by such low  $^{187}\text{Os}/^{188}\text{Os}$  (Horan et al., 2009). The sub-chondritic  $^{187}\text{Os}/^{188}\text{Os}$  of both of these meteorites requires time-integrated low-Re/Os, which cannot be accounted for by impactor additions. NWA 4801 and NWA 4590 are coarse-grained (crystal sizes are generally 1–2 mm) crystalline samples that are probable cumulates and thermally annealed rocks, respectively; these meteorites contain olivines with Mg# < 60 (where Mg# = 100 Mg/[Mg + Fe<sup>total</sup>]; supplementary materials), and they are not residual mantle materials. The relatively high total HSE abundances and low  $^{187}\text{Os}/^{188}\text{Os}$  of NWA 4590 and NWA 4801, therefore, are features incorporated prior to or during crystallization of their parental magmas on the APB.

NWA 4801 and NWA 4590 are also characterized by low-Pd, relative to other HSE (e.g., [Pd/Os]<sub>N</sub> = 0.06 to 0.75, where N denotes normalization to Orgueil values reported by Horan et al., 2003). It is unlikely that low-Pd/Os in these meteorites result from solid-metal liquid-metal partitioning, as proposed for partially differentiated achondrites (e.g., brachinites and ureilites; Day et al., 2012b; Rankenburg et al., 2008). In contrast to NWA 4801, ureilites and brachinites show no evidence for enhanced Re/Os fractionations of the magnitude required to explain the sub-chondritic  $^{187}\text{Os}/^{188}\text{Os}$  of NWA 4801. In addition, no iron meteorites exist with such low long-term Re/Os (e.g., Horan et al., 1992; Smoliar et al., 1996).

We examine three possible scenarios that may generate low-Re/Os signatures in NWA 4801 and NWA 4590. The first scenario is that oxygen fugacity played a major role in Re/Os fractionation within planetary basalts. Birck and Allègre (1994) first explored this hypothesis on planetary basalts using measured Os abundances,  $^{187}\text{Os}/^{188}\text{Os}$  isotope compositions, and inferred Re abundances (e.g., Re\*) for a number of achondrites and lunar rocks. Experimental studies of HSE partitioning indicate that magmas produced under relatively oxidizing conditions (cf., angrites and terrestrial basalts) will have elevated Re<sup>6+</sup>/Re<sup>4+</sup> (e.g., Brenan, 2008; Ertel et al., 2001) compared with magmas produced under relatively reducing conditions (cf., lunar and eucrite magmas). These valence-state variations lead to higher Re/Os at a given Os abundance in oxidized magmas. This model predicts that angrites will crystallize with elevated Re/Os with respect to chondrites, producing supra-chondritic Os-isotope compositions over extended time periods. However, low time-integrated Re/Os for NWA 4801 and NWA 4590 cannot be explained by high-*f*O<sub>2</sub>, and other angrites do not conform to this model.

Secondly, it is possible that the relatively high-*f*O<sub>2</sub> conditions inferred for quenched-angrite-magma genesis could have led to loss of Re through magmatic degassing as oxidized or halogenated complexes (cf., Crowe et al., 1987; Day et al., 2010b; Hinkley et al., 1999; Sun et al., 2003 and references therein). However, angrites define broad positive correlations between (Os, Ir, Ru, Pt, Pd, Re)/Yb, compared with Re abundances (supplementary materials). These characteristics contrast with (Os, Ir, Ru, Pt, Pd, Re)/Yb systematics reported for sub-aerially erupted alkali lavas from the Canary Islands (Day et al., 2010b), suggesting that magmatic degassing of Re was an unlikely process on the APB.

A third model involves multiple melt-depletion events in the APB. In this context, low-Re/Os in these angrites may be inherited from a magmatic source region that experienced prior-melt removal (cf., Schaefer et al., 2002 for a terrestrial analog). This model involves selective depletion of the HSE that are generally considered to behave incompatibly in sulfide-bearing

silicate–melt systems (e.g., Re, Pt, and Pd) versus HSE abundances that are considered to behave more compatibly (Os, Ir, and Ru; e.g., Barnes et al., 1985). Prior depletion of angrite magma reservoirs is broadly supported by the generation of younger quenched-angrites with high-Re/Os and chondritic-relative REE. Although the analogy to models of multiple melt generation events on Earth may account for the low-Re/Os in younger slowly-cooled angrites with fractionated REE, it does not account for the presence of kamacite + tetrataenite in NWA 4801, or the moderate degrees of HSE fractionation compared to magmatic products of the Earth, Moon, and Mars (supplementary materials). Furthermore, there is no obvious correlation between angrite HSE abundances and indices of melt-depletion (e.g., Mg/Fe; supplementary materials).

A positive slope between Re abundances and ratios of Os and Ir to Re and Yb suggests that Os and Ir behave moderately-incompatibly during angrite-magma genesis (supplementary materials). Furthermore, the presence of metal in the crystallizing assemblage of some angrites exerted a major influence on angrite HSE abundances and magmatic HSE fractionation on the APB. Kleine et al. (2012) recently suggested that W behaves compatibly with respect to Hf, and FeNi metals identified in this study may account for this Hf–W behavior during angrite-magma genesis. The presence of kamacite and tetrataenite as late-crystallizing phases in NWA 4801 is contradictory to the relatively high- $f_{O_2}$  conditions thought to account for the silicate assemblage of quenched-angrites ( $\log f_{O_2} = IW + 1$  to  $+2$ ; e.g., Jurewicz et al., 1993; McKay et al., 1994; Longhi, 1999). The dynamics of melt generation and magma processing that control HSE behavior during the genesis of some angrite-magmas probably differ from the sulfide-dominated systems of the Moon, Mars, and Earth (+/– Os–Ir alloys inferred for some high-degree, S-under-saturated terrestrial melts and residues; e.g., Luguet et al., 2007; Puchtel et al., 2004; supplementary materials). However, the low measured Re/Os in NWA 4801 and NWA 4590 are best explained by multiple melt- or sulfide-removal episodes within the APB prior to the crystallization of these magma products.

#### 4.5. Metal–silicate differentiation in, and late accretion to, the angrite parent body

Angrite portions least affected by the addition of exogenous chondritic materials (Table 1) contain HSE abundances substantially in excess of those predicted for magmas generated from a mantle stripped of its HSE by low-pressure metal–silicate differentiation, where  $D^{\text{metal/silicate}}$  values are on the order of  $\geq 10^4$  (e.g., Borisov and Palme, 1997). Two scenarios of angrite origin can explain the range of HSE abundances and Os-isotope compositions. The first model involves the addition of HSE to the APB mantle following core formation, but before complete solidification. The second model entails incomplete core formation and retention of some metal in the silicate portion of the APB.

Two important pieces of evidence suggest that the APB differentiated and developed a metallic core  $\sim 2$  Ma after the formation of some of the earliest CAIs: 1) angrites were derived from source regions with supra-chondritic Hf/W (Kleine et al., 2012; Markowski et al., 2007); and 2) paleomagnetic constraints suggest the presence of an early-formed core dynamo (Weiss et al., 2008). Mineralogical studies (refer to section 3.1 and supplementary materials) show that early crystallizing phases in angrite magmas are relatively Mg-rich. This behavior is similar to that reported in silicate systems of the Earth, Moon, and Mars for which broad MgO–HSE fraction trends have been reported (e.g., Brandon et al., 2012; Day et al., 2007; Warren et al., 1989, 1999). To estimate angrite mantle HSE characteristics we

compared angrite MgO (not shown), MgO+FeO\* (where all Fe is assumed to occur as Fe<sup>2+</sup>), HSE abundances, and Pt/Os values to those determined for other planetary magma products (cf., supplementary materials). The presence of FeNi metal in NWA 4801 leads to a preferred model of angrite mantle HSE abundance estimates based on comparisons with MgO+FeO\*. The least contaminated quenched-angrites and NWA 4590 overlap data fields of lunar, martian, and terrestrial basalts. However, NWA 4801 contains elevated HSE concentrations relative to terrestrial and martian magma products with similar MgO+FeO\*. These MgO+FeO\* to HSE abundance variations, combined with initial <sup>187</sup>Os/<sup>188</sup>Os within the chondritic range (Table 1), suggest that the silicate mantle of the APB contained chondritic proportions of HSE with variable absolute abundances. The source region(s) of younger quenched-angrites contained the lowest HSE abundances of  $\leq 0.0002 \times \text{CI-chondrite}$ , analogous to, or lower than, lunar mantle HSE concentrations (Day et al., 2007). In contrast, the source region(s) of older slowly-cooled NWA 4801 and NWA 4590 contained HSE concentrations  $\geq 0.008 \times \text{CI-chondrite}$ , which may be in excess of estimates for terrestrial and martian systems (e.g., Becker et al., 2006; Brandon et al., 2012; Warren et al., 1999). Widely varying abundance estimates of HSE in the APB magma source regions are consistent with predictions derived from comparison of HSE abundances with MgO contents (not shown) and Pt/Os ratios (supplementary materials). These observations strongly support silicate–metal equilibration, followed by variable amounts of late accretion additions to the APB.

#### 4.6. Protracted accretion and core–mantle–crust differentiation in the early Solar System

Current compositional and chronological data for angrites, combined with existing spectral analogs (cf., Scott and Bottke, 2011; supplementary materials), lead to a preferred model in which the APB is viewed as a small differentiated body (Fig. 5) that may represent a planetary pre-cursor, and our results are discussed in this context.

Studies of terrestrial, lunar, and martian samples have shown that variable proportions of HSE were added to the mantles of these planetary bodies (approximately 0.02% of the lunar and 0.4% of the terrestrial and martian mantle masses; Brandon et al., 2000, 2012; Chou, 1978; Day et al., 2007; Walker, 2009). The mass proportions of impact contributions to the Earth, Moon, and Mars, and the relative proportions of impact-flux between the Earth and Moon cannot be accounted for by gravitational attraction forces alone (e.g., Day et al., 2007; Morgan et al., 2001). Recent models of stochastic accretion involving large impacts (Bottke et al., 2010) may explain the relative proportions of impact additions indicated by lunar, terrestrial, and martian mantle HSE abundance estimates. In this context, angrites provide evidence of significant additions of chondritic HSE to mantles of planetary pre-cursors in the early Solar System (prior to 4.53 Ga; Dale et al., 2012), showing that post-core formation accretion is a protracted process that likely began early in Solar System history (cf., Day et al., 2012a). Variable quantities of HSE in chondritic proportions in angrite magma source regions also imply inefficient mixing of accreted materials at the APB scale. The variable absolute HSE abundances of angrites do not support the single estimate of HSE abundances in the APB mantle inferred from a smaller dataset for angrites (cf. Dale et al., 2012). Angrites, instead provide further evidence for wide-spread late accretion to bodies ranging from asteroids to planets, but also indicate that late accretion additions likely do not scale in a simplistic manner to the size or oxidation state of the parent body.

## Acknowledgements

We thank A. D. Patchen and R. D. Ash for their assistance with EMP and LA-ICP-MS analyses, respectively. We are grateful for the provision of a polished section of Sahara 99555 by C. Floss, and for whole-rock fragments of Angra dos Reis, D'Orbigny, and NWA 1296 from the Smithsonian Institution Museum of Natural History, A. Ruzicka and M. Hutson, and T. Kleine, respectively. A. J. Irving is thanked for his general assistance with the allocation of angrite material. Insightful comments by Klaus Keil, an anonymous reviewer, and the Editor, Tim Elliott, are greatly appreciated. This work was supported by NASA Cosmochemistry grants NNX08AG54G, NNX10AG94G, NNX12AH75G and NNX09AB92G to LAT, RJW, JMDD, and CRN respectively. Additional support for this work was provided by the University of Tennessee Planetary Geosciences Institute.

## Appendix A. Supporting information

Supplementary data associated with this article can be found in the online version at [10.1016/j.epsl.2012.08.006](http://dx.doi.org/10.1016/j.epsl.2012.08.006).

## References

- Amelin, Y., 2008. U–Pb ages of angrites. *Geochim. Cosmochim. Acta* 72, 221–232.
- Amelin, Y., Connelly, J., Zartman, R.E., Chen, J.H., Göpel, C., Neymark, L.A., 2009. Modern U–Pb chronometry of meteorites: Advancing to higher time resolution reveals new problems. *Geochim. Cosmochim. Acta* 73 (17), 5212–5223.
- Anders, E., Grevesse, N., 1989. Abundances of the elements – Meteoritic and solar. *Geochim. Cosmochim. Acta* 53, 197–214.
- Baker, J., Bizzarro, M., Wittig, N., Connelly, J., Haack, H., 2005. Early planetesimal melting from an age of 4.5662 Gyr for differentiated meteorites. *Nature* 436, 1127–1131.
- Barnes, S.J., Naldrett, A.J., Gorton, M.P., 1985. The origin and fractionation of platinum group elements in terrestrial magmas. *Chem. Geol.* 53, 303–323.
- Becker, H., Horan, M.F., Walker, R.J., Gao, S., Lorand, J.-P., Rudnick, R.L., 2006. Highly siderophile element composition of the Earth's primitive upper mantle: constraints from new data on peridotite massifs and xenoliths. *Geochim. Cosmochim. Acta* 70, 4528–4550.
- Birck, J.-L., Allègre, C.J., 1994. Contrasting Re/Os magmatic fractionation in planetary basalts. *Earth Planet. Sci. Lett.* 124, 139–148.
- Borisov, A., Palme, H., 1997. Experimental determination of the solubility of platinum in silicate melts. *Geochim. Cosmochim. Acta* 61, 4349–4357.
- Botke, W.F., Walker, R.J., Day, J.M.D., Nesvorný, D., Elkins-Tanton, L., 2010. Stochastic Late Accretion to Earth, the Moon, and Mars. *Science* 330, 1527–1530.
- Brandon, A.D., Walker, R.J., Morgan, J.W., Goles, G.C., 2000. Re–Os isotopic evidence for early differentiation of the Martian mantle. *Geochim. Cosmochim. Acta* 64 (23), 4083–4095.
- Brandon, A.D., Puchtel, I.S., Walker, R.J., Day, J.M.D., Irving, A.J., Taylor, L.A., 2012. Evolution of the martian mantle inferred from  $^{187}\text{Re}$ – $^{187}\text{Os}$  isotope and highly siderophile element abundance systematics of shergottite meteorites. *Geochim. Cosmochim. Acta* 76, 206–235.
- Brenan, J.M., 2008. Re–Os fractionation by sulphide melt–silicate melt partitioning: A new spin. *Chem. Geol.* 248, 140–165.
- Chou, C.-L., 1978. Fractionation of siderophile elements in the Earth's upper mantle. In: *Proceedings of Ninth Lunar and Planetary Science Conference*, 219–230.
- Clayton, R.N., 2003. Oxygen isotopes in meteorites. In: *Treatise on Geochemistry*, vol. 1, Elsevier Ltd., pp. 129–142.
- Connelly, J.N., Bizzarro, M., Thrane, K., Baker, J.A., 2008. The Pb–Pb age of angrite SAH99555 revisited. *Geochim. Cosmochim. Acta* 72 (19), 4813–4824.
- Crockett, J.H., Keays, R.R., Hsieh, S., 1967. Precious metal abundances in some carbonaceous and enstatite chondrites. *Geochim. Cosmochim. Acta* 31, 1615–1623.
- Crowe, B.L., Finnegan, D.L., Zoller, W.H., Boynton, W.V., 1987. Trace element geochemistry of volcanic glasses and particles from the 1983–1984 eruptive episodes of Kilauea volcano. *J. Geophys. Res.* 92, 13708–13714.
- Dale, C.W., Burton, K.W., Greenwood, R.C., Gannoun, A., Wade, J., Wood, B.J., Pearson, D.G., 2012. Late accretion on the earliest planetesimals revealed by the highly siderophile elements. *Science* 336, 72–75.
- Day, J.M.D., Pearson, D.G., Taylor, L.A., 2007. Highly siderophile element constraints on accretion and differentiation of the Earth–Moon system. *Science* 315, 217–219.
- Day, J.M.D., Ash, R.D., Liu, Y., Bellucci, J.J., Rumble, D.I.I.I., McDonough, W.F., Walker, R.J., Taylor, L.A., 2009. Early formation of evolved asteroidal crust. *Nature* 457, 179–182.
- Day, J.M.D., Walker, R.J., James, O.B., Puchtel, I.S., 2010a. Osmium isotope and highly siderophile element systematics of the lunar crust. *Earth Planet. Sci. Lett.* 289, 595–605.
- Day, J.M.D., Pearson, D.G., MacPherson, C.G., Lowry, D., Carrecedo, J.-C., 2010b. Evidence for distinct proportions of oceanic crust and lithosphere in HIMU-type mantle beneath El Hierro and La Palma, Canary Islands. *Geochim. Cosmochim. Acta* 74, 6565–6589.
- Day, J.M.D., Walker, R.J., Qin, L., Rumble, D.I.I.I., 2012a. Late accretion as a natural consequence of planetary growth. *Nature Geosci.*, <http://dx.doi.org/10.1038/NNGEO1527>.
- Day, J.M.D., Walker, R.J., Ash, R.D., Liu, Y., Rumble, D.I.I.I., Irving, A.J., Goodrich, C.A., Tait, K., McDonough, W.F., Taylor, L.A., 2012b. Origin of felsic achondrites Graves Nunataks 06128 and 06129 and ultramafic brachinites and brachinite-like achondrites by partial melting of volatile-rich primitive parent bodies. *Geochim. Cosmochim. Acta* 81, 94–128.
- Ertel, W., O'Neill, H.St.C., Sylvester, P.J., Dingwell, D.B., Spettel, B., 2001. The solubility of rhenium in silicate melts: implications for the geochemical properties of rhenium at high temperatures. *Geochim. Cosmochim. Acta* 65, 2161–2170.
- Fischer-Gödde, M., Becker, H., Wombacher, F., 2010. Rhodium, gold and other highly siderophile element abundances in chondritic meteorites. *Geochim. Cosmochim. Acta* 74 (1), 356–379.
- Floss, C., Crozaz, G., McKay, G., Mikouchi, T., Killgore, M., 2003. Petrogenesis of angrites. *Geochim. Cosmochim. Acta* 67 (24), 4775–4789.
- Franchi, I.A., 2008. Oxygen isotopes in asteroidal materials. *Rev. Mineral. Geochem.* 68, 345–397.
- Greenwood, R.C., Franchi, I.A., Jambon, A., Buchanan, P.C., 2005. Widespread magma oceans on asteroidal bodies in the early Solar System. *Nature* 435, 916–918.
- Herr, W., Herpers, U., Michel, R., Abdel Rassoul, A.A., Woelfle, R., 1971. Search for rhenium isotopic anomalies in lunar surface material by neutron bombardment. In: *Proceedings of 2<sup>nd</sup> Lunar Science Conference*, 1337–1341.
- Hinkley, T.K., Lamothe, P.J., Wilson, S.A., Finnegan, D.L., Gerlach, T.M., 1999. Metal emissions at Kilauea and a suggested revision of the estimated worldwide metal output by quiescent degassing volcanoes. *Earth Planet. Sci. Lett.* 170, 315–325.
- Horan, M.F., Morgan, J.W., Walker, R.J., 1992. Rhenium–osmium isotope constraints on the age of iron meteorites. *Science* 255, 1118–1121.
- Horan, M.F., Walker, R.J., Morgan, J.W., Grossman, J.N., Rubin, A., 2003. Highly siderophile elements in chondrites. *Chem. Geol.* 196, 5–20.
- Horan, M.F., Alexander, C.M.O.'D., Walker, R.J., 2009. Highly siderophile element evidence for early solar system processes in components from ordinary chondrites. *Geochim. Cosmochim. Acta* 73, 6984–6997.
- Humayun, M., Irving, A.J., Kuehner, S.M., 2007. Siderophile elements in metal-rich angrite NWA 2999. In: *Lunar and Planetary Science Conference*, abstract #1221.
- Jambon, A., Barrat, J.-A., Boudouma, O., Fonteilles, M., Badia, D., Göpel, C., Bohn, M., 2005. Mineralogy and petrology of the angrite Northwest Africa 1296. *Meteorit. Planet. Sci.* 40 (3), 361–375.
- Jambon, A., Boudouma, O., Fonteilles, M., Le Guillou, C., Badia, D., Barrat, J.-A., 2008. Petrology and mineralogy of the angrite Northwest Africa 1670. *Meteorit. Planet. Sci.* 43 (11), 1783–1795.
- Jones, J.H., Drake, M.J., 1986. Geochemical constraints on core formation in the Earth. *Nature* 322, 221–228.
- Jones, J.H., Neal, C.R., Ely, J.C., 2003. Signatures of the highly siderophile elements in SNC meteorites and Mars: a review and petrologic synthesis. *Chem. Geol.* 196, 21–41.
- Jurewicz, A.J.G., Mittlefehldt, D.W., Jones, J.H., 1993. Experimental partial melting of the allende CV and Murchison (CM) chondrites and the origin of asteroidal basalts. *Geochim. Cosmochim. Acta* 57, 2123–2139.
- Kallemeyn, G.W., Wasson, J.T., 1981. The compositional classification of chondrites: I. The carbonaceous chondrite groups. *Geochim. Cosmochim. Acta* 45, 1217–1230.
- Keil, K., 2012. Angrites, a small but diverse suite of ancient, silica-undersaturated volcanic–plutonic mafic meteorites, and the history of their parent asteroid. *Chemie der Erde*, <http://dx.doi.org/10.1016/j.chemer.2012.06.002>, in press.
- Kimura, K., Lewis, R.S., Anders, E., 1974. Distribution of gold and rhenium between nickel–iron and silicate melts. *Geochim. Cosmochim. Acta* 38, 683–781.
- Kleine, T., Touboul, M., Bourdon, B., Nimmo, F., Mezger, K., Plame, H., Jacobsen, S.B., Yin, Q.-Z., Halliday, A.N., 2009. Hf–W chronology of the accretion and early evolution of asteroids and terrestrial planets. *Geochim. Cosmochim. Acta* 73, 5150–5188.
- Kleine, T., Hans, U., Irving, A.J., Bourdon, B., 2012. Chronology of the angrite parent body and implications for core formation in protoplanets. *Geochim. Cosmochim. Acta* 84 (1), 186–203.
- Kurat, G., Varela, M.E., Brandstätter, F., Weckwerth, G., Clayton, R.N., Webber, H.W., Schultz, L., Wäscher, M.A., Nazarov, M.A., 2004. D'Orbigny: A non-igneous angritic achondrite? *Geochim. Cosmochim. Acta* 68 (8), 1901–1921.
- Longhi, J., 1999. Phase equilibrium constraints on angrite petrogenesis. *Geochim. Cosmochim. Acta* 63, 573–585.
- Lugmair, G.W., Galer, S.J.G., 1992. Age and isotopic relationships among the angrites Lewis Cliff 86010 and Angra dos Reis. *Geochim. Cosmochim. Acta* 56 (4), 1673–1694.

- Luguet, A., Shirey, S.B., Lorand, J.-P., Horan, M.F., Carlson, R.W., 2007. Residual platinum-group minerals from highly depleted harzburgites of the Lherz massif (France) and their role in HSE fractionation of the mantle. *Geochim. Cosmochim. Acta* 71, 3082–3097.
- Mann, U., Frost, D.J., Rubie, D.C., Becker, H., Audétat, A., 2012. Partitioning of Ru, Rh, Pd, Re, Ir, and Pt between liquid metal and silicate at high pressures and high temperatures – Implications for the origin of highly siderophile element concentrations in the Earth's mantle. *Geochim. Cosmochim. Acta* 84, 593–613.
- Markowski, A., Quitte, G., Kleine, T., Halliday, A., Bizzarro, M., Irving, A.J., 2007. Hf–W chronometry of angrites and the earliest evolution of planetary bodies. *Earth Planet. Sci. Lett.* 262, 214–229.
- McKay, G., Le, L., Wagstaff, J., Crozaz, G., 1994. Experimental partitioning of rare earth elements and strontium: Constraints on petrogenesis and redox conditions during crystallization of Antarctic angrite Lewis Cliff 86010. *Geochim. Cosmochim. Acta* 58 (13), 2911–2919.
- Michel, R., Herpès, U., Kulus, H., Herr, W., 1972. Isotopic anomalies in lunar rhenium. *Proc. 3<sup>rd</sup> Lunar Sci. Conf.*, 1917–1925.
- Mitchell, R.H., Keays, R.R., 1981. Abundance and distribution of gold, palladium and iridium in some spinel and garnet lherzolites: implications for the nature and origin of precious metal rich intergranular components in the upper mantle. *Geochim. Cosmochim. Acta* 45, 2425–2445.
- Mittlefehldt, D.W., Lindstrom, M.M., 1990. Geochemistry and genesis of the angrites. *Geochim. Cosmochim. Acta* 54, 3209–3218.
- Mittlefehldt, D.W., Killgore, M., Lee, M.T., 2002. Petrology and geochemistry of D'Orbigny, geochemistry of Sahara 99555, and the origin of angrites. *Meteorit. Planet. Sci.* 37, 345–369.
- Mittlefehldt, D.W., Clayton, R.N., Drake, M.J., Righter, K., 2008. Oxygen isotopic composition and chemical correlations in meteorites and the terrestrial planets. *Rev. Mineral. Geochem.* 68, 399–427.
- Morgan, J.W., Lovering, J.F., 1967. Rhenium and osmium abundances in some igneous and metamorphic rocks. *Earth Planet. Sci. Lett.* 3, 219–224.
- Morgan, J.W., Wandless, G.A., Petrie, R.K., Irving, A.J., 1981. Composition of the Earth's upper mantle-1. Siderophile trace elements in ultramafic nodules. *Tectonophysics* 75, 47–67.
- Morgan, J.W., Walker, R.J., Brandon, A.D., Horan, M.F., 2001. Siderophile elements in Earth's upper mantle and lunar breccias: Data synthesis suggests manifestations of the same late influx. *Meteorit. Planet. Sci.* 36 (9), 1257–1275.
- Nyquist, L.E., Kleine, T., Shih, C.-Y., Reese, Y.D., 2009. The distribution of short-lived radioisotopes in the early solar system and the chronology of asteroid accretion, differentiation, and secondary mineralization. *Geochim. Cosmochim. Acta* 73 (17), 5115–5136.
- O'Neill St., H., Dingwell, C., Borisov, D.B., Spettel, A., Palme, H., B., 1995. Experimental petrochemistry of some highly siderophile elements at high temperatures, and some implications for core formation and the mantle's early history. *Chem. Geol.* 120, 255–273.
- Peucker-Ehrenbrink, B., Jahn, B.-M., 2001. Rhenium-osmium isotope systematics and platinum group element concentrations: loess and the upper continental crust. *Geochim. Geophys. Geosys.* 2 2001GC000172.
- Puchtel, I.S., Humayun, M., Campbell, A.J., Sproule, R.A., Leshner, C.M., 2004. Platinum group element geochemistry of komatiites from the Alexo and Pyke Hill areas, Ontario, Canada. *Geochim. Cosmochim. Acta* 68 (6), 1361–1383.
- Quitte, G., Markowski, A., Latkoczy, C., Gabriel, A., Pack, A., 2010. Iron-60 Heterogeneity and Incomplete Isotope Mixing in the Early Solar System. *Astro. Phys. J.* 720 (2), 1215–1224.
- Rankenburg, K., Humayun, M., Brandon, A.D., Herrin, J.S., 2008. Highly siderophile elements in ureilites. *Geochim. Cosmochim. Acta* 72, 4642–4659.
- Rehkämper, M., Halliday, A.N., Fitton, J.G., Lee, D.-C., Wieneke, M., Arndt, N.T., 1999. Ir, Ru, Pt, and Pd in basalts and komatiites: New constraints for the geochemical behaviour of the platinum-group elements in the mantle. *Geochim. Cosmochim. Acta* 63 (22), 3915–3934.
- Riches A.J.V., Day J.M.D., Walker R.J., Liu Y., Taylor L.A., 2010 Variable highly siderophile element abundances and sub-chondritic  $^{187}\text{Os}/^{188}\text{Os}$  in the angrite parent body. In: 73rd Annual Meeting of the Meteoritical Society, abstract #5210.
- Riches, A.J.V., Liu, Y., Day, J.M.D., Puchtel, I.S., Rumble, D.I.I.I., McSween, H.Y., Walker, R.J., Taylor, L.A., 2011. Petrology and geochemistry of Yamato 984028: A cumulate lherzolitic shergottite with affinities to Y 000027, Y 000047, and Y 000097. *Polar Sci.* <http://dx.doi.org/10.1016/j.polar.2010.04.009>.
- Ringwood, A.E., 1966. Chemical evolution of the terrestrial planets. *Geochim. Cosmochim. Acta* 30, 41–104.
- Rivkin, A.S., Trilling, D.E., Thomas, C.A., DeMeo, F., Spahr, R.B., Binzel, R.P., 2007. Composition of the L5 Mars Trojans: Neighbors, not siblings. *Icarus* 192, 434–441.
- Schaefer, B.F., Turner, S., Parkinson, I.J., Rogers, N.W., Hawkesworth, C.J., 2002. Evidence for recycled Archaean oceanic mantle lithosphere in the Azores plume. *Nature* 420, 304–307.
- Scott, E.R.D., Bottke, W.F., 2011. Impact histories of angrites, eucrites, and their parent bodies. *Meteorit. Planet. Sci.* 46 (12), 1878–1887.
- Smoliar, M.I., Walker, R.J., Morgan, J.W., 1996. Re-Os ages of Group IIA, IIIA, IVA, and IVB Meteorites. *Science* 271 (5252), 1099–1102.
- Sun, W., Bennett, V.C., Eggins, S.M., Kamenetsky, V.S., Arculus, R.J., 2003. Enhanced mantle-to-crust rhenium transfer in undegassed arc magmas. *Nature* 422, 294–297.
- Trilling, D.E., Rivkin, A.S., Stansberry, J.A., Spahr, T.B., Crudo, R.A., Davies, J.K., 2007. Albedos and diameters of three Mars Trojan asteroids. *Icarus* 192, 442–447.
- van Acken, D., Brandon, A.D., Humayun, M., 2011. High-precision osmium isotopes in enstatite and Rumuruti chondrites. *Geochim. Cosmochim. Acta* 75 (14), 4020–4036.
- Varela, M.E., Kurat, G., Zinner, E., Métrich, N., Brandstätter, F., Natflos, T., Sylvester, P., 2003. Glasses in the D'Orbigny angrite. *Geochim. Cosmochim. Acta* 67 (24), 5027–5046.
- Varela, M.E., Kurat, G., Zinner, E., Hoppe, P., Natflos, T., Nazarov, M.A., 2005. The non-igneous genesis of angrites: Support from trace-element distribution between phases of D'Orbigny. *Meteorit. Planet. Sci.* 40 (3), 409–430.
- Wakita, H., Schmitt, R.A., 1970. Lunar Anorthosites: Rare-Earth and Other Elemental Abundances. *Science* 170 (3961), 969–974.
- Walker, R.J., 2009. Highly siderophile elements in the Earth, Moon and Mars: Update and implications for planetary accretion and differentiation. *Chem Erde* 69, 101–125.
- Walker, R.J., Horan, M.F., Morgan, J.W., Becker, H., Grossman, J.N., Rubin, A.E., 2002. Comparative  $^{187}\text{Re}$ - $^{187}\text{Os}$  systematics of chondrites: Implications regarding early solar system processes. *Geochim. Cosmochim. Acta* 66 (23), 4187–4201.
- Walker, R.J., Horan, M.F., Shearer, C.K., Papike, J.J., 2004. Low abundances of highly siderophile elements in the lunar mantle: evidence for prolonged late accretion. *Earth Planet. Sci. Lett.* 244, 399–413.
- Warren, P.H., Jerde, E.A., Kallemeyn, G.W., 1989. Lunar meteorites: siderophile element contents, and implications for the composition and origin of the Moon. *Earth Planet. Sci. Lett.* 91 (3–4), 245–260.
- Warren, P.H., Kallemeyn, G.W., Kyte, F.T., 1999. Origin of planetary cores: evidence from highly siderophile elements in martian meteorites. *Geochim. Cosmochim. Acta* 63 (13–14), 2105–2122.
- Weiss, B.P., Berdahl, J.S., Elkins-Tanton, L., Stanley, S., Lima, E.A., Carporzen, L., 2008. Magnetism on the angrite parent body and the early differentiation of planetesimals. *Science* 322, 713–716.

## 1 **Supplementary Material**

### 2 **A1. Extended methods**

3 Polished sections of angrites and small-chips mounted in 1-inch epoxy mounts were used  
4 for petrographic investigations and *in situ* studies of mineral compositions. Interior portions of  
5 meteorites were disaggregated and ground to fine powders with limited force, and major- and  
6 trace-element abundances were measured on the first set of powder fractions prepared. Prior to  
7 disaggregation of samples, the alumina mortar and pestle was thoroughly cleaned and leached  
8 using dilute HCl, abraded with pure quartz powder, thoroughly rinsed with ultra-pure water, and  
9 dried between uses.

#### 10 *A1.1 Major- and trace-element compositions of minerals*

11 The major-element compositions of minerals of five angrites were determined using a  
12 *Cameca* SX-100 electron microprobe (EMP) at the University of Tennessee. Pyroxene, olivine,  
13 and oxide phases were measured using a beam size of  $\leq 5 \mu\text{m}$ , a 20nA beam current, and an  
14 accelerating potential of 15Kv. Feldspar, phosphate, and sulfide were analyzed with a beam size  
15 of  $\leq 5 \mu\text{m}$ , a 10nA beam current, and an accelerating potential of 15Kv. Counting times were 20  
16 to 30 seconds for all elements, and standard PAP corrections were applied to all analyses.  
17 Precision and accuracy were monitored with natural and synthetic standards at intervals during  
18 each analytical session, and drift was within counting error. Detection limits ( $3\sigma$  above  
19 background) are typically  $<0.03$  wt. % for  $\text{SiO}_2$ ,  $\text{TiO}_2$ ,  $\text{Al}_2\text{O}_3$ ,  $\text{MgO}$ ,  $\text{CaO}$ , and  $<0.04$ – $0.15$  wt. %  
20 for  $\text{FeO}$ ,  $\text{MnO}$ ,  $\text{Cr}_2\text{O}_3$ ,  $\text{NiO}$ ,  $\text{Na}_2\text{O}$ ,  $\text{K}_2\text{O}$ ,  $\text{SO}_2$ ,  $\text{P}_2\text{O}_5$ ,  $\text{Y}_2\text{O}_3$ ,  $\text{V}_2\text{O}_3$ , F, and Cl.

21 Trace-element abundances of pyroxene, feldspar, and phosphate were measured using a  
22 *New Wave Research* UP213 (213 nm) Nd:YAG laser-ablation system, coupled to a

23 *ThermoFinnigan* Element 2 ICP-MS, at the University of Notre Dame and at the University of  
24 Maryland. In addition, these instruments were used at the University of Maryland to determine  
25 the highly-siderophile-element abundances of constituent minerals of NWA 4931.

26 During trace-element analyses a laser repetition rate of 5 to 7 Hz and energy densities of  
27 1.8 to 2.5 J/cm<sup>2</sup> were employed, and each grain was analyzed with spot sizes ranging from 15 to  
28 80 µm. Data were acquired across a mass range of <sup>45</sup>Sc to <sup>238</sup>U, and samples were ablated in a  
29 pure He atmosphere then mixed with argon before entering the plasma (*c.f.*, Günther and  
30 Heinrich, 1999). Th/ThO production was ~0.07 % for all analytical sessions. Backgrounds on  
31 the ICP-MS sample gas were collected for ~20 s followed by ~40 s of laser ablation of the  
32 sample. Washout time between analyses was >2 min. Trace-element data were collected in  
33 time-resolved mode so that effects of inclusions, mineral zoning and laser beam penetration  
34 could be evaluated. LA-ICP-MS data were processed using the Glitter and LAM-TRACE  
35 software at the University of Notre Dame and Maryland, respectively. Detection limits across  
36 the <sup>45</sup>Sc to <sup>238</sup>U mass-range were generally within the 10-100 ppb range and represent the  
37 standard deviations (3σ level) calculated based on the average background ion signals measured.

38 The NIST 610 and 612 glass standards were used for external calibration purposes  
39 during LA-ICP-MS trace-element analyses, and two MIP-DING standards, kl2-g and ml3b-g,  
40 and the Durango apatite were analyzed as unknowns to assess accuracy and reproducibility at the  
41 University of Notre Dame (Supplementary Table S1). Minor- and trace-element reproducibility  
42 of the standard was generally better than 5 % (RSD), Elemental abundances of kl2-g and ml3b-g  
43 were generally within error (1σ<sub>stdev</sub>) of the preferred values, and reproducibility was generally  
44 better than 5 % (RSD). At the University of Maryland, replicate LA-ICP-MS analyses of the  
45 BIR-1g glass standard run at intervals during analytical sessions yielded an external precision of

46 better than 3 % ( $1\sigma$  relative standard deviation) for all measured element compositions of  
47 silicates and phosphates.

48 Replicate LA-ICP-MS analyses of the University of Toronto JB Sulfide standard and the  
49 in-house Filomena iron meteorite standard run at intervals during analysis of highly-siderophile-  
50 element abundances yielded an external precision of better than 1 % ( $1\sigma$  relative standard  
51 deviation) for highly-siderophile-element abundances. Calcium oxide wt. % values determined  
52 by EMP analysis were employed as the internal standard for LA-ICP-MS analyses, whereas  
53 measurements of highly-siderophile-element abundances were normalized to the Fe-content  
54 determined by EMP analysis.

#### 55 *A1.2 Major- and trace-element compositions of bulk-rocks*

56 Approximately 10 mg of powder was fused using a Mo-strip heater in an N<sub>2</sub> atmosphere  
57 to form a glass-bead on which major-element abundances were determined by electron  
58 microprobe (EMP). Multiple analytical points (generally  $n > 25$ ) were measured using a 10  $\mu\text{m}$   
59 beam size, 10 nA beam current, and an accelerating voltage of 15 kV (*c.f.*, Riches et al. 2011).

60 For trace-element analysis ~50 mg of powder was digested with a 4:1 solution of HF-  
61 HNO<sub>3</sub> in Paar bombs that were heated in an oven for ~48 hours at 180°C. Following digestion,  
62 samples were evaporated to dryness before equilibrating with 6N HCl. HCl solutions were dried  
63 down and the residue was then redissolved in 2 % HNO<sub>3</sub>. Trace-element abundances were  
64 measured by ICP-MS using a *ThermoFinnigan* Element 2 at the University of Maryland.  
65 Analyses were standardized against three reference materials (BIR-1, BHVO-1, and BCR-2) that  
66 were measured at the beginning and the end of each analytical run. In addition, three reference  
67 materials were analyzed as “unknowns” every 6-10 samples (BIR-1, BHVO-1, and BCR-2) in

68 order to monitor instrumental drift and to assess the external reproducibility and accuracy  
69 (Supplementary Table S2). Reproducibility of the reference materials was generally better than 3  
70 % (RSD), and element abundances were generally within error ( $1\sigma_{\text{stdev}}$ ) of the recommended  
71 values. During solution analyses, detection limits ( $3\sigma$  above background) were typically <1ppb  
72 for all elements.

### 73 *A1.3 Further details pertaining to Re-Os and HSE analyses*

74 With the exception of analytical grade  $\text{CCl}_4$ , all reagents used in sample digestion and  
75 element pre-concentration procedures were multiply Teflon-distilled. Samples were sealed in 12  
76 mL borosilicate Carius tubes, with isotopically enriched multi-element spikes ( $^{99}\text{Ru}$ ,  $^{106}\text{Pd}$ ,  $^{185}\text{Re}$ ,  
77  $^{190}\text{Os}$ ,  $^{191}\text{Ir}$ , and  $^{194}\text{Pt}$ ) and ~6.5 to 9 mL of acid mixture (5 parts 12 M HCl and 8 parts purged  
78 16M  $\text{HNO}_3$ ). Samples were digested at a maximum temperature of 270°C over a minimum  
79 heating period of 72 hrs. Osmium was triply extracted from the acid-solution in  $\text{CCl}_4$  (Cohen  
80 and Waters, 1996), and back-extracted from the solvent in concentrated HBr, followed by  
81 microdistillation purification (Birck et al., 1997). The remaining HSE were recovered from  
82 residual acid solutions using an anion exchange separation technique modified from Becker et al.  
83 (2006). After evaporating to incipient dryness, sample solutions were equilibrated in ~6 mL of  
84 1M HCl, and residual solids were separated by centrifugation. The supernatant liquid was  
85 loaded onto ~1.6 mL of pre-cleaned AG 1-X8 (100-200#) anion exchange resin. The matrix was  
86 eluted using 1M HCl, 1N HF-HCl and 0.8N  $\text{HNO}_3$ , prior to collection of Ir, Pt, Ru and Re in  
87 concentrated  $\text{HNO}_3$  and collection of Pd in warm concentrated HCl.

88 During measurement of osmium isotope compositions with the *ThermoFisher* Triton at  
89 the University of Maryland, possible contributions from Re were monitored at masses 233  
90 ( $^{185}\text{ReO}_3^-$ ), 249 ( $^{185}\text{ReO}_4^-$ ), and 251 ( $^{187}\text{ReO}_4^-$ ). Signal at mass 233 was always found to be

91 negligible (<5 cps), so Os isotope ratios were not corrected for Re interference. Raw data was  
92 processed offline to account for oxygen speciation (using  $^{18}\text{O}/^{16}\text{O}$  and  $^{17}\text{O}/^{16}\text{O}$  values of Nier,  
93 1950), an iterative fractionation correction using a  $^{192}\text{Os}/^{188}\text{Os}$  ratio of 3.08271 (Shirey and  
94 Walker, 1998), a  $^{190}\text{Os}$  spike subtraction, and blank contribution corrections. External precision  
95 of  $^{187}\text{Os}/^{188}\text{Os}$  during the analytical campaign was determined by individual measurements of 3.5  
96 to 35 pg of the UMCP Johnson and Matthey Os-standard, and was better than  $\pm 0.2\%$   
97 ( $^{187}\text{Os}/^{188}\text{Os} = 0.11380 \pm 20$ ,  $n = 13$ ;  $2\sigma_{\text{stdev}}$ ).

98 Abundances of the HSE determined by ICP-MS employed an offline fractionation  
99 correction using the deviation from the mean value of standards measured on the day of analysis,  
100 relative to the natural isotopic ratio for the element. During analyses, instrumental drift, and  
101 oxide ( $\text{UO}^+/\text{U} = 0.05\%$ ) and element interferences were negligible.

## 102 **A2. Supplementary results**

### 103 *A2.1 Extended petrography and mineralogy*

104 All of the studied angrites contain variable proportions of; early-crystallized anorthite; zoned  
105 pyroxenes that display increasing Al and Ti and decreasing  $\text{Mg}/(\text{Mg}+\text{Fe})$  from core to rim; zoned  
106 olivine/kirschsteinite that co-crystallized with pyroxene; minor late-stage magnetite or  
107 ulvöspinel; sulfide (typically troilite); and silico-phosphates. Some samples also contain  
108 merrillite, kamacite (NWA 4801 and NWA 4931), tetrataenite (NWA 4801), rhönite (NWA  
109 4590), and baddelyite (e.g., Angra dos Reis). Goethite and celsian, potentially resulting from  
110 terrestrial alteration, occur in some of the angrites (e.g., Angra dos Reis; NWA 4801; NWA  
111 4931).

112 Textural characteristics of quenched-angrites (D'Orbigny and Sahara 99555) indicate that  
113 anorthite crystallized early and was followed by zoned pyroxene, which displays decreasing Mg#  
114 (where  $Mg\# = 100Mg/(Mg+Fe^{total})$ ), and increasing Ti- and Al-content from core to rim. Zoned  
115 olivines appear broadly coincident with zoned pyroxenes, and show pronounced core-to-rim  
116 compositional variation of increasing Fe- and Ca-content toward olivine rims. Late-stage phases  
117 include kirschsteinite, ulvöspinel, troilite and silico-phosphate. Angrites with ages that are  
118 resolvably younger than quenched-angrites (Appendix B) are generally coarser-grained (up to  
119 3mm), and individual samples generally contain phase assemblages similar to that of quenched-  
120 angrites. However, constituent minerals of slowly-cooled angrites cover a more restricted range  
121 of major-element compositions than quenched-angrites (Figs. A2 to A4).

122 NWA 4931 is paired with NWA 2999 and is texturally anomalous; NWA 4931 is dominated  
123 by poikilitic Ca-bearing olivine enclosing lesser amounts of anhedral anorthite, fassaitic  
124 pyroxene, and hercynitic spinel. In addition, NWA 4931 contains variable proportions of altered  
125 metal grains (now present as goethite and magnetite up to 400  $\mu\text{m}$  at the maximum dimension).  
126 Altered metals also infill narrow veinlets (<30  $\mu\text{m}$  wide) throughout the sample. Kamacite (<30  
127  $\mu\text{m}$  in diameter) is rare and occurs in the interior portions of altered grains.

128 Core-to-rim traverses of pyroxenes generally reveal increasing Fe-contents, decreasing Sc-  
129 abundances, increasing La-concentrations (not shown), and increasing chondrite-normalized  
130 La/Yb values toward the rim. In detail, abundances of Ti and Zr determined by laser ablation are  
131 generally below 15000 and 200 ppm, respectively, and this result differs from that reported for  
132 ion-probe measurements of trace-element abundances in pyroxene rims of quenched angrites.  
133 The reasons for these differences remain unclear, and may potentially reflect differences in; 1)  
134 the volume of sample analyzed in these two *in situ* studies, or 2) instrument specific calibration  
135 procedures.

136 Angrite olivines cover a range of Fe- and Mn-contents that define a fractionation line  
137 with a slope broadly similar to that reported for terrestrial samples (Fig. A4). However, Fe- and  
138 Mn-contents of fassaitic angrite pyroxenes delineate a fractionation line with a shallower slope  
139 than reported for Earth. Angrite spinels, ranging from Mg-Al spinel to  $\text{ülvöspinel}$  compositions,  
140 have relatively low V- and Cr-contents (generally  $<0.2$  wt. %  $\text{V}_2\text{O}_3$ , and  $<3$  wt. %  $\text{Cr}_2\text{O}_3$ ;  
141 Appendix B) compared to chromites of Graves Nunatak (GRA) 06128/9 ( $\sim 2.2$  to  $2.7$  wt. %  
142  $\text{V}_2\text{O}_3$ , and up to  $38.4$  wt. %  $\text{Cr}_2\text{O}_3$ ; Day et al., 2009; Shearer et al., 2010), and spinel-group  
143 minerals of martian basalts (e.g., up to  $1.14$   $\text{V}_2\text{O}_3$ , and up to  $\sim 57$  wt. %  $\text{Cr}_2\text{O}_3$ ; e.g., Goodrich et  
144 al., 2003; Herd, 2006).

145 Constituent minerals of angrites display a number of common trace-element  
146 characteristics (Fig. A5); 1) early-formed anorthites are characterized by large positive Eu-  
147 anomalies ( $[\text{Eu}/\text{Eu}^*]_{\text{N}} = 88.4$  to  $137$ ; where  $[\text{Eu}^* = (\text{Sm}+\text{Gd})/2]$  and N denotes normalization to  
148 CI-chondrite values of Anders and Grevesse, 1989); 2) pyroxenes are light-rare-earth-element  
149 (LREE)-depleted ( $[\text{La}/\text{Yb}]_{\text{N}} = 0.27$  to  $0.95$ ), with minor negative Eu-anomalies ( $[\text{Eu}/\text{Eu}^*]_{\text{N}} =$   
150  $0.39$  to  $0.97$ ); 3) olivine grains are LREE-depleted ( $[\text{La}/\text{Yb}]_{\text{N}} = 0.03$  to  $0.11$ ), and the absolute  
151 abundance of REE increases with increasing Ca-content; and 4) phosphates have negative Eu-  
152 anomalies ( $[\text{Eu}/\text{Eu}^*]_{\text{N}} = 0.59$  to  $0.66$ ) and are LREE-enriched ( $[\text{La}/\text{Yb}]_{\text{N}} = 14.1$  to  $18.0$ ).  
153 Abundances of Ti, Zr, Y, and Sc, and  $[\text{La}/\text{Yb}]_{\text{N}}$  values determined for pyroxenes by laser  
154 ablation (LA-) ICP-MS analyses cover a range broadly analogous to that reported from an ion-  
155 probe study of quenched-angrites (Floss et al., 2003; Fig. A6).

## 156 A2.2 Reconstructed bulk-rock trace-element compositions

157 Reconstructed bulk-rock compositions of Angra dos Reis and NWA 4801 are reported in  
158 the appendix B along with the calculation methodology. With the exception of Cr, La, Zr, and

159 Hf, trace-element abundances of the reconstructed Angra dos Reis bulk-rock are generally within  
160 3 to 16 % of the measured bulk-powder fraction. In addition, the shape of the chondrite-  
161 normalized reconstructed bulk-rock trace-element pattern is similar to that of the measured bulk-  
162 rock powder. In contrast, reconstructed trace-element abundances of NWA 4801 are consistently  
163 elevated (20 to 60 % for Cr, Sm, Eu, Gd, HREE, Zr, Hf, and U; 121 to 310 % for LREE, Nd, and  
164 Th) when compared to the two measured bulk-rock powder fractions. Differences between  
165 reconstructed and measured bulk-rock trace-element compositions for relatively coarse-grained  
166 Angra dos Reis and NWA 4801 can be attributed to moderate differences in the modal  
167 proportions studied in polished sections compared to bulk-rock portions crushed for wet-  
168 chemical analyses, most especially pyroxene and incompatible-element-rich phosphates.

### 169 **A3. Extended literature review**

170 Angrites are silica under-saturated, have supra-chondritic Ca/Al (e.g., Mittlefehldt and  
171 Lindstrom, 1990), and are characterized by  $\epsilon^{50}\text{Ti}$  distinct from those of lunar and terrestrial  
172 materials (Zhang et al., 2012). Coexisting Al-Ti-rich pyroxenes, Ca-rich olivines, anorthite and  
173 other mineralogical characteristics of Angrites may indicate their genesis under relatively  
174 oxidizing conditions ( $\log f\text{O}_2$  IW+2; e.g., Mittlefehldt et al., 2002; Floss et al., 2003; Jambon et  
175 al., 2005, 2008), and Angrite  $\delta^{56}\text{Fe}$  compositions which overlap with the terrestrial range may  
176 provide evidence to support the relatively oxidized nature of these meteorites (after Wang et al.,  
177 2012). Angrites are also characterized by: 1) low Rb/Sr; and 2) bulk-rock and internal isochrons  
178 that define low initial  $^{87}\text{Sr}/^{86}\text{Sr}$  ( $\leq$ BABI; the basaltic achondrite best initial). Combined, these  
179 results suggest that the APB may have experienced volatile-element depletion early in its history  
180 (Lugmair and Galer, 1992; Wasserburg et al., 1977).

181 The identity of the APB is unknown, but it is likely a body similar in size to, or smaller  
182 than, Vesta (Scott and Bottke, 2011). Spectral reflectance data suggest that the km-sized Mars

183 Trojan asteroid, Eureka, provides a close spectral match to angrites (Rivkin et al., 2007; Trilling  
184 et al., 2007). Some authors have suggested that angrites may even be derived from Mercury's  
185 earliest crust (e.g., Irving et al., 2005, 2006; Kuehner et al., 2006), but this hypothesis remains  
186 contentious (*cf.*, Scott and Bottke, 2011 and references therein). In addition, the mineralogical  
187 assemblage of angrites contrasts to preliminary results from MESSENGER (MErcury Surface,  
188 Space ENvironment, GEochemistry and Ranging), which suggest that the Mercurian crust is S-  
189 rich, has low Fe- and Ti-abundances, and is derived from a relatively reduced mantle that may  
190 have high C-content (e.g., McCubbin et al., 2012; Weider et al., 2011; Zolotov et al., 2011).

191

**Table A1:** Trace-element composition of geochemical reference materials measured by LA-ICP-MS during this study.

	kl2-g				ml3b-g				Durango apatite		
	average	RSD (%)	Preferred	$\Delta S-R(\%)$	average	RSD (%)	Preferred	$\Delta S-R(\%)$	average	RSD (%)	LA-ICP <sup>1</sup>
<b>Sc (ppm)</b>	29.0(4)	1.44	31.8(9)	8.78	28.2(3)	0.96	32(2)	10.8	0.6(1)	20.9	-
<b>Ti</b>	15087(145)	0.96	15347(540)	1.70	13940(390)	2.79	12769(540)	9.17	460(24)	5.28	-
<b>Cr</b>	254(9)	3.62	294(27)	13.5	195(5)	2.68	177(23)	10.4	-	-	-
<b>Mn</b>	917(216)	26.9	1278(70)	28.3	1480(21)	1.41	1316(70)	12.4	101(4)	4.33	84(4)
<b>Co</b>	35(2)	6.09	41(2)	15.5	51.2(5)	0.93	41(4)	24.3	12(2)	17.8	-
<b>Ni</b>	134(4)	2.70	112(5)	19.6	176(6)	3.38	107(9)	64.8	-	-	3.2(4)
<b>Ga</b>	35(2)	4.38	20(1)	76.3	32.9(8)	2.33	19(2)	67.6	2.19(6)	2.72	-
<b>Rb</b>	7.6(8)	10.8	8.7(4)	12.2	6.8(4)	6.10	5.8(2)	17.2	-	-	0.13(2)
<b>Sr</b>	343(13)	3.79	356(8)	3.67	320(15)	4.79	312(4)	2.52	727(40)	5.57	475(12)
<b>Y</b>	22.4(2)	1.07	25(1)	12	16.8(7)	4.36	23.9(7)	29.7	972(69)	7.13	1232(42)
<b>Zr</b>	132(3)	2.60	152(5)	13.1	89(4)	4.31	122(3)	26.9	1.0(3)	24.2	1.4(2)
<b>Nb</b>	15.1(1)	0.69	15.0(5)	0.96	9.1(4)	4.27	8.6(2)	5.54	0.03(1)	22.9	-
<b>Ba</b>	113(1)	0.89	123(5)	8.20	87(2)	1.89	80(2)	8.82	17.6(8)	4.27	19.4(9)
<b>La</b>	12.7(2)	1.82	13.1(2)	3.38	8.1(2)	2.88	8.9(1)	9.42	-	-	4140(144)
<b>Ce</b>	30.5(9)	3.13	32.4(7)	5.79	27(1)	4.63	23.1(3)	15.3	-	-	4464(185)
<b>Pr</b>	4.5(3)	5.43	4.6(1)	1.59	3.24(7)	2.19	3.43(6)	5.44	-	-	455(18)
<b>Nd</b>	20.5(4)	1.93	21.6(4)	5.00	14.8(2)	1.06	16(2)	11.6	1342(46)	3.43	1538(64)
<b>Sm</b>	5.4(1)	2.06	5.54(9)	1.74	4.0(2)	3.95	4.75(7)	15.4	205(7)	3.41	229(14)
<b>Eu</b>	2.3(3)	14.0	1.92(4)	20.0	1.54(2)	1.14	1.67(2)	7.58	14.6(7)	4.61	16.3(6)
<b>Gd</b>	5.5(3)	4.97	5.9(2)	6.42	3.7(2)	5.74	5.3(2)	30.4	297(16)	5.42	247(13)
<b>Tb</b>	1.1(1)	12.9	0.89(3)	20.9	0.65(1)	2.02	0.80(2)	18.6	31(2)	5.23	31(2)
<b>Dy</b>	5.0(2)	3.16	5.2(1)	4.79	3.56(6)	1.69	4.84(7)	26.4	157(10)	6.21	189(10)
<b>Ho</b>	1.2(2)	15.7	0.96(2)	21.9	0.62(1)	1.69	0.91(2)	32.0	31(2)	6.06	39(2)
<b>Er</b>	2.6(2)	6.20	2.54(7)	2.62	1.78(2)	0.93	2.44(5)	27.0	88(7)	8.23	108(5)
<b>Tm</b>	0.5(2)	36.7	0.331(9)	62.4	0.22(2)	8.07	0.324(7)	32.6	10.6(8)	7.28	13.5(6)
<b>Yb</b>	2.3(2)	8.54	2.10(5)	7.94	1.6(1)	6.30	2.06(4)	24.5	57(4)	7.00	71(3)
<b>Lu</b>	0.4(1)	23.8	0.285(9)	50.8	0.21(3)	14.9	0.286(6)	27.9	6.2(4)	6.16	8.3(3)
<b>Hf</b>	3.6(1)	3.49	3.9(1)	8.91	2.2(2)	9.28	3.22(8)	31.7	-	-	-
<b>Ta</b>	1.4(4)	27.7	0.96(2)	41.2	0.50(4)	7.95	0.56(1)	10.2	0.03(1)	41.8	-
<b>Pb</b>	2.2(4)	19.6	2.1(1)	7.12	1.50(7)	4.70	1.38(7)	8.45	1.03(6)	5.42	0.78(7)
<b>Th</b>	1.3(3)	22.4	1.02(3)	29.0	0.46(1)	2.60	0.55(1)	16.3	294(12)	4.07	387(9)
<b>U</b>	1.1(6)	49.6	0.55(2)	102	0.52(4)	7.60	0.44(2)	16.9	14.6(5)	3.52	11(1)

Values in brackets are the standard deviation corresponding to the least figure/decimal cited, and are calculated from four measurements of the geochemical reference material, the associated relative standard deviation (RSD) is shown and recommended abundance values for the reference materials are listed for comparison. Deviation from the preferred value (\*) is given by  $\Delta S-R = 100 * (\text{sample/reference} - 1)$ . Preferred values of KL2-g and ml3b-g were reported by Jochum et al., 2006. The measured values of the Durango apatite are compared to the average and  $1\sigma_{\text{stdev}}$  values reported for LA-ICP-MS analyses of Durango apatite standards reported by (1) Simonetti et al., 2008.

**Table A2:** Trace-element abundances of geochemical reference materials measured in solution by ICP-MS during the analytical period of this study.

	BIR-1				BHVO-1				BCR-2			
	average	RSD (%)	Preferred	$\Delta S-R(\%)$	average	RSD (%)	Preferred	$\Delta S-R(\%)$	average	RSD (%)	Preferred	$\Delta S-R(\%)$
<b>Li (ppm)</b>	3.1(1)	3.7	3.2(2)	2.03	4.67(1)	0.13	4.6(2)	1.58	9.6(1)	1.49	9(2)	6.15
<b>Sc</b>	42.98(1)	0.01	43(2)	0.04	31.5(8)	2.56	31(2)	0.36	34.8(9)	2.55	33(2)	5.37
<b>V</b>	325(2)	0.67	319(18)	1.97	318(2)	0.56	318(15)	0.42	438(10)	2.32	416(14)	5.40
<b>Cr</b>	423(4)	0.90	391(15)	8.18	289(2)	0.63	287(15)	0.04	16.9(4)	2.58	18(2)	6.11
<b>Co</b>	53.6(6)	0.62	52(3)	3.16	44.95(5)	0.12	45(3)	0.12	38.8(1)	3.31	37(3)	4.93
<b>Ni</b>	172(3)	1.93	166(7)	3.45	119.4(6)	0.49	118(6)	0.94	18(1)	6.57	18(1)	3.89
<b>Cu</b>	117.2(9)	0.75	119(8)	1.50	149(1)	0.82	137(9)	0.59	21(2)	9.35	21(1)	3.81
<b>Rb</b>	0.221(2)	0.80	0.2(1)	10.4	9.21(3)	0.36	9.2(2)	0.09	53.6(1)	0.24	46.9(1)	14.2
<b>Sr</b>	98.8(3)	0.25	109(2)	9.32	388.5(5)	0.13	396(1)	0.39	344(3)	0.77	340(3)	1.13
<b>Y</b>	15.70(1)	0.68	15.6(9)	0.89	26.95(3)	0.12	26(2)	0.18	38.6(2)	0.56	37(2)	4.34
<b>Zr</b>	13.85(4)	0.28	14.0(1)	1.06	176.100(4)	0.00	174(9)	0.09	199.7(3)	0.16	184(1)	8.52
<b>Nb</b>	0.555(2)	0.34	0.55(5)	0.84	19.60(4)	0.23	19(2)	0.33	13.1(2) \	1.71	12.6(4)	3.81
<b>Mo</b>	0.037(1)	3.7	0.07	47.3	1.02(3)	3.37	1.0(2)	0.46	274(3)	1.01	250(20)	9.81
<b>Cs</b>	0.0054(1)	2.01	0.007(3)	22.6	0.0956(1)	0.13	0.101(8)	0.39	1.19(1)	0.75	1.1(1)	8.42
<b>Ba</b>	7.01(5)	0.73	7.14	1.78	129.8(7)	0.54	133(1)	0.16	699(2)	0.28	677(2)	3.26
<b>La</b>	0.630(5)	0.73	0.62(2)	2.41	15.5(1)	0.63	15.5(1)	0.62	26.2(1)	0.40	24.9(2)	5.41
<b>Ce</b>	1.97(2)	0.99	1.92(8)	2.47	38.17(7)	0.18	38.1(2)	0.73	55.4(4)	0.66	52.9(2)	4.66
<b>Pr</b>	0.370(5)	1.24	0.37(2)	0.02	5.18(4)	0.72	5.4(2)	0.51	6.92(2)	0.15	6.7(1)	2.31
<b>Nd</b>	2.47(3)	1.01	2.38(1)	3.93	24.9(1)	0.42	24.7(1)	1.00	30.2(2)	0.50	28.7(1)	5.38
<b>Sm</b>	1.15(2)	1.89	1.12(2)	2.51	6.163(2)	0.04	6.12(3)	0.37	6.92(2)	0.25	6.58(2)	5.23
<b>Eu</b>	0.53(1)	1.32	0.53	0.80	2.06(2)	0.79	2.09(2)	0.10	2.09(4)	1.78	1.96(1)	6.65
<b>Gd</b>	1.75(3)	1.71	1.87(4)	6.37	6.30(2)	0.39	6.33(6)	0.27	7.20(9)	1.25	6.75(3)	6.74
<b>Tb</b>	0.37(1)	2.0	0.36(3)	1.61	0.95(1)	0.71	0.96(6)	0.38	1.12(1)	0.77	1.07(3)	4.87
<b>Dy</b>	2.63(5)	1.89	2.51	4.63	5.26(2)	0.30	5.31(3)	0.24	6.62(8)	1.24	6.41(5)	3.22
<b>Ho</b>	0.61(1)	1.41	0.56(5)	8.64	1.01(1)	0.57	0.98(5)	0.04	1.39(1)	0.45	1.28(3)	8.69
<b>Er</b>	1.75(3)	1.78	1.66	5.21	2.56(1)	0.52	2.55(2)	0.16	3.83(5)	1.26	3.66(1)	4.59
<b>Tm</b>	0.27(1)	2.06	0.25(3)	8.60	0.347(1)	0.35	0.33(3)	0.34	0.570(3)	0.52	0.54(4)	5.63
<b>Yb</b>	1.71(4)	2.11	1.65	3.51	2.03(1)	0.37	2.00(3)	0.44	3.54(6)	1.69	3.38(2)	4.70
<b>Lu</b>	0.26(1)	2.06	0.25(2)	5.13	0.2858(4)	0.14	0.270(5)	0.65	0.535(4)	0.69	0.503(9)	6.38
<b>Hf</b>	0.61(1)	2.36	0.582(4)	5.01	4.36(3)	0.59	4.5(2)	0.30	5.1(1)	2.16	4.9(1)	3.63
<b>Ta</b>	0.0450(3)	0.75	0.0357(4)	25.9	1.205(1)	0.10	1.2(2)	0.38	0.84(2)	1.89	0.74(2)	13.7
<b>W</b>	0.019(9)	46.9	0.07	3.64	0.216(4)	1.78	0.21(2)	7.09	0.50(2)	3.14	-	-
<b>Pb</b>	3.0(1)	3.18	3.1(3)	2.71	2.08(2)	1.12	2.4(9)	0.19	11.4(4)	3.16	11(1)	3.17
<b>Th</b>	0.032(1)	2.62	0.032(4)	1.49	1.244(2)	0.16	1.23(7)	0.67	6.0(2)	3.52	5.7(5)	5.37
<b>U</b>	0.0093(3)	2.92	0.010(1)	7.17	0.421(3)	0.75	0.409(2)	0.31	1.77(6)	3.37	1.7(2)	4.84

Values in brackets are the standard deviation corresponding to the least figure/decimal cited, and are calculated from four measurements of the geochemical reference material for data obtained in this study. The associated relative standard deviation (RSD) is shown, and deviation from the preferred value is given by  $\Delta S-R = 100 * (\text{sample/reference} - 1)$ . Preferred values of BIR-1, BHVO-1, and BHVO-2 were taken from those compiled on the GEOREM database.

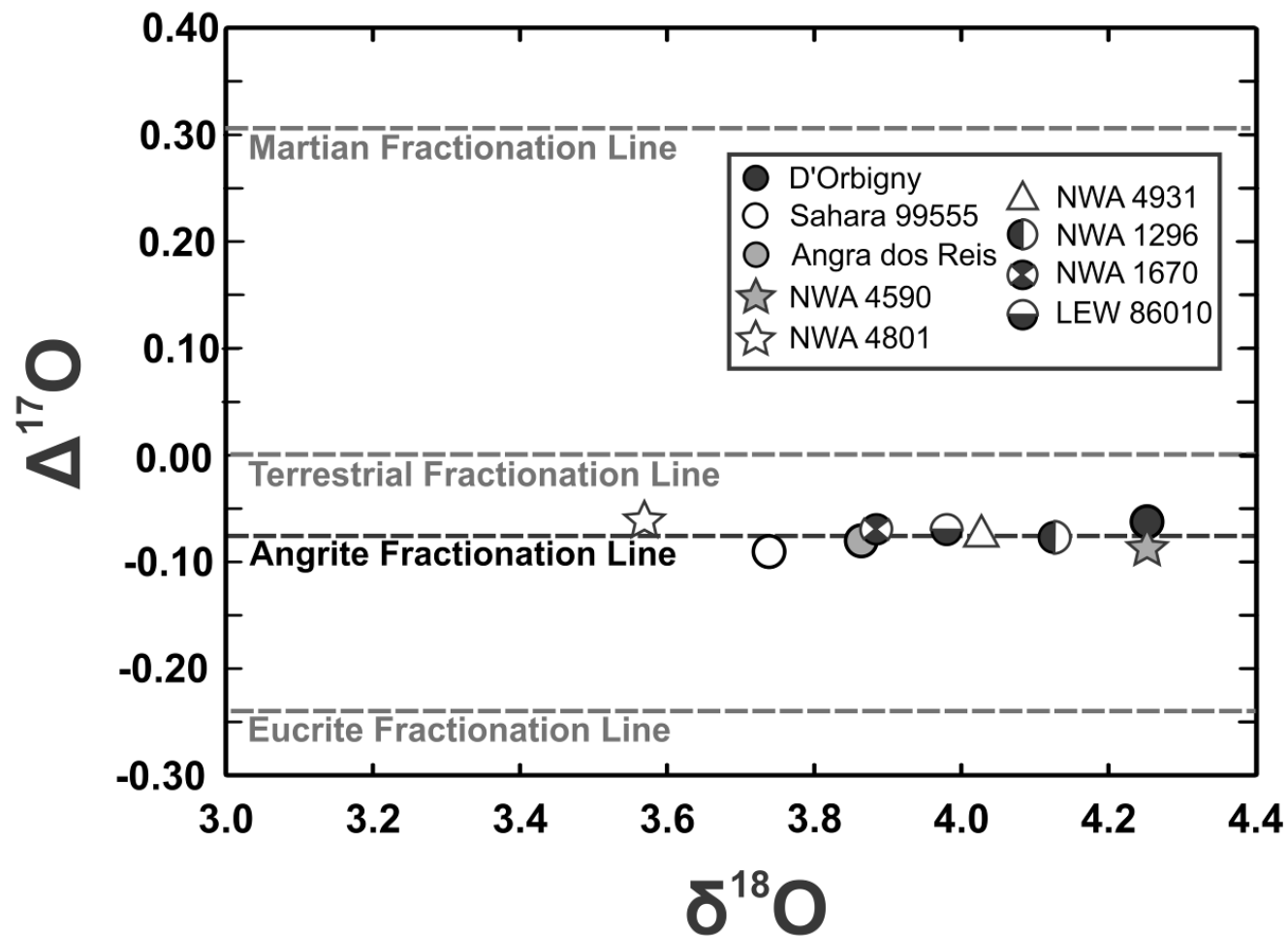
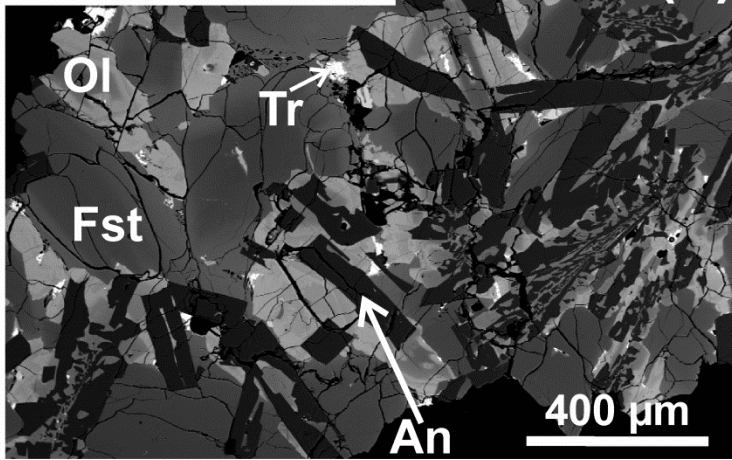
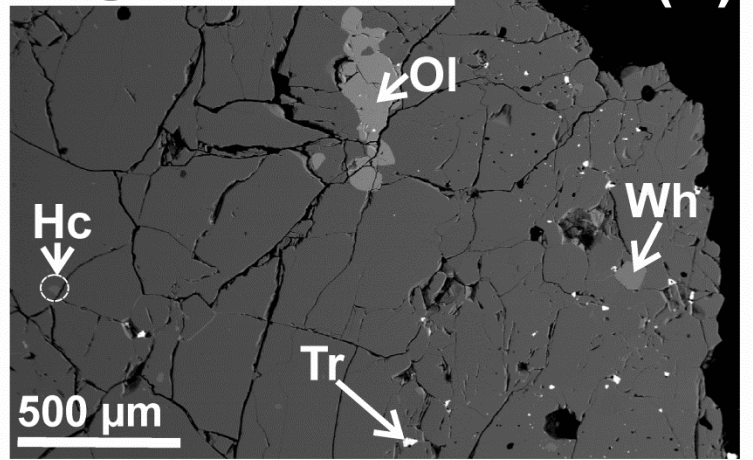


**Figure A1:** Oxygen isotope composition of angrites after Greenwood et al. (2005), with values for Sahara 99555, NWA 4801, NWA 4590, and NWA 4931 reported by Bischoff et al. (2000), and available in the meteoritical bulletins 90 and 92, assuming that NWA 4931 has an oxygen isotope composition identical to its pair, NWA 2999.

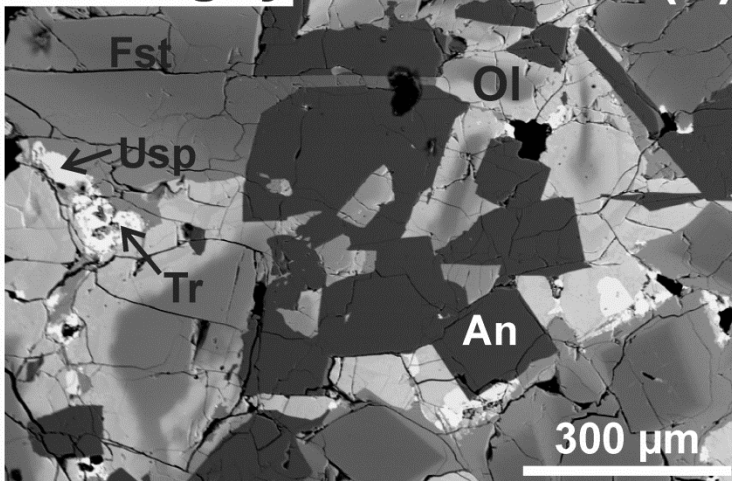
**Sahara 99555 (a)**



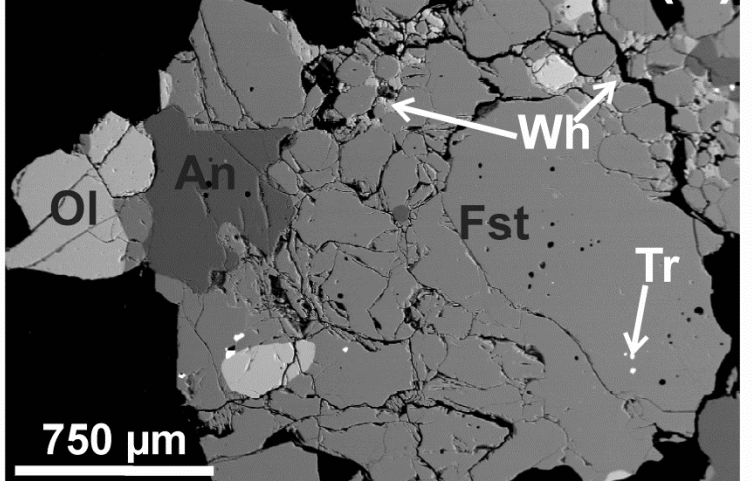
**Angra dos Reis (b)**



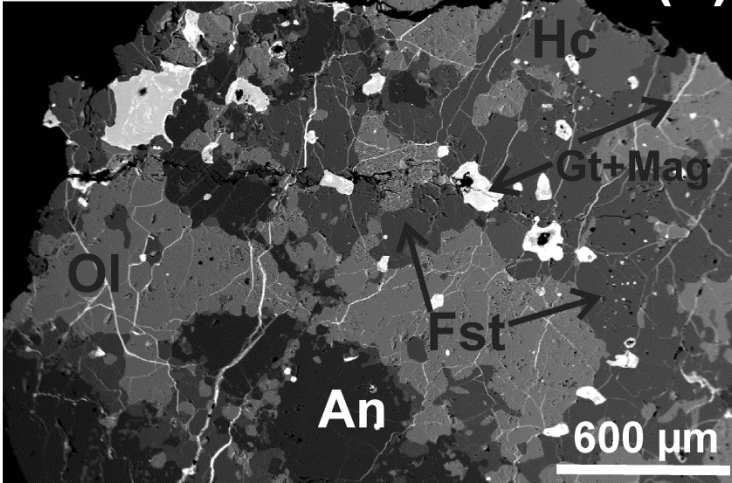
**D'Orbigny (c)**



**NWA 4801 (d)**



**NWA 4931 (e)**



**NWA 4590 (f)**

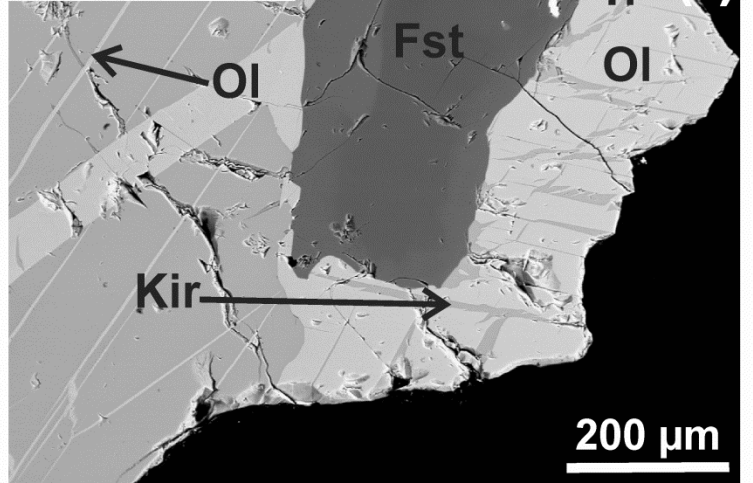


**Figure A2:** Back-scattered electron images of portions of the studied polished sections illustrating textural diversity within the Angrite suite. Sahara 99555 (a) and D'Orbigny (c) show hypidiomorphic and subophitic textures, respectively, and contain zoned olivines and fassaite. In contrast, Angra dos Reis (b) has a relatively equilibrated texture with poikilitic fassaites in the right of the image enclosing troilite and whitlockite, and some 120° pyroxene triple junctions evident in this section. NWA 4801 (d) lacks exsolution textures analogous to those preserved in NWA 4590 (f). NWA 4931 (e) is composed of coarse-grained poikilitic olivine and fassaite with symplectic features adjacent to anorthites in the bottom of this view. An = anorthite. Fst = fassaite. Gt = goethite. Hc = hercynite. Mag = magnetite. Kir = kirschsteinite. Ol = olivine. Tr = troilite. Usp = ulvöspinel. Wh = whitlockite.

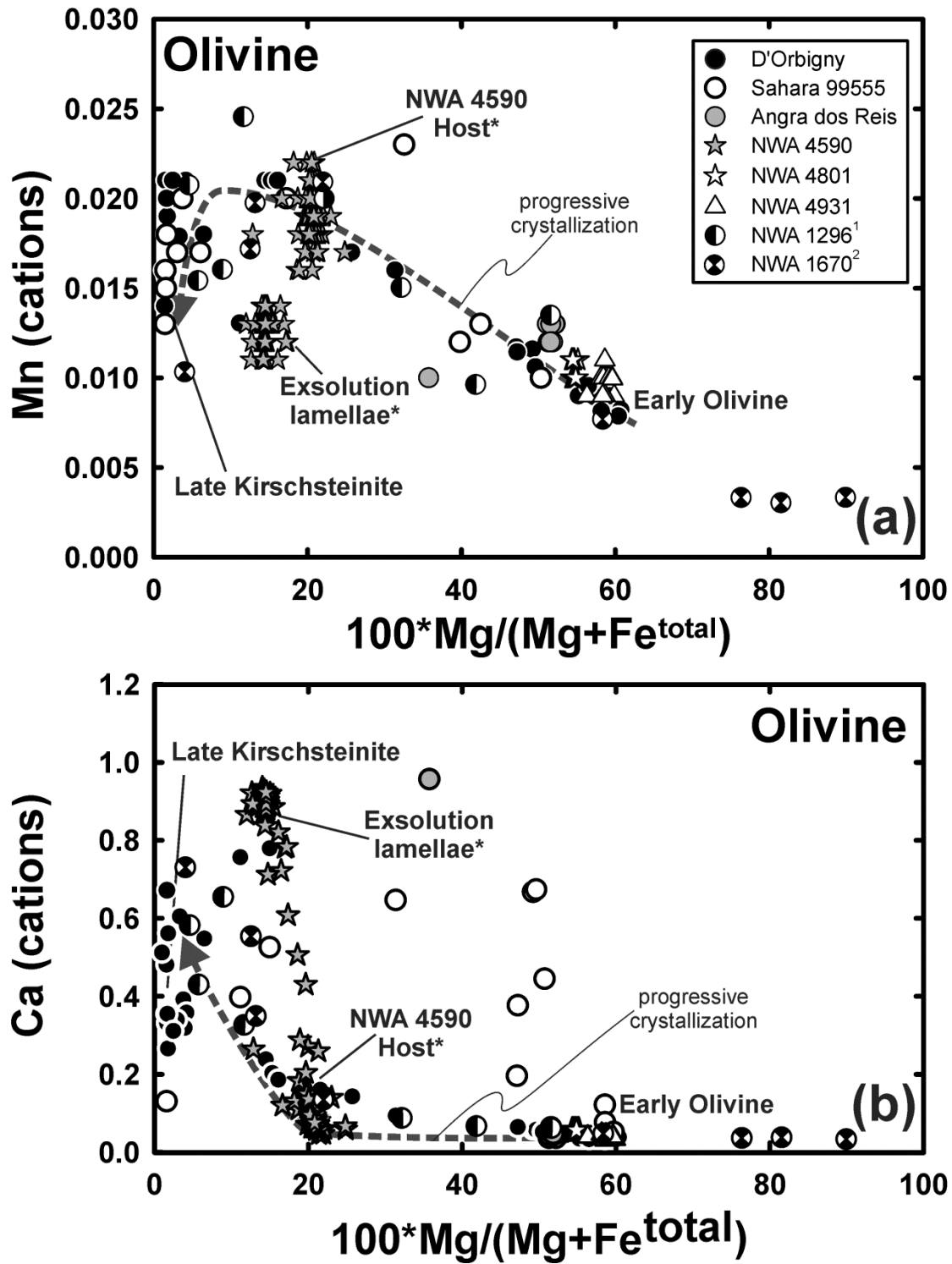


**Figure A2:** Major-element compositions of olivines. Olivines of NWA 1296 and NWA 1670 were reported by (1) Jambon et al. (2005), and (2) Jambon et al. (2008).

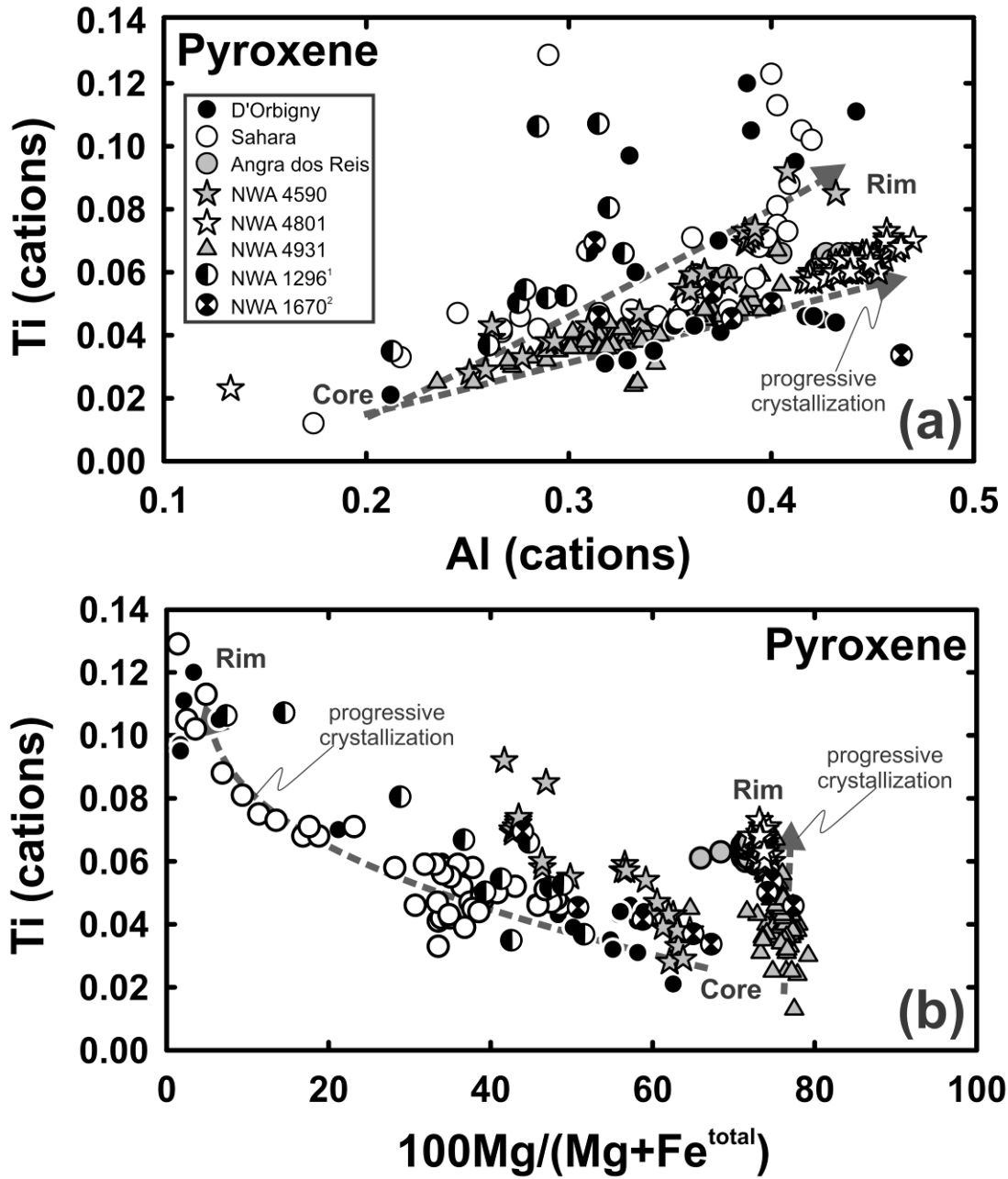


**Figure A3:** Major-element compositions of pyroxenes. Pyroxene compositions of NWA 1296 and NWA 1670 were determined by (1) Jambon et al. (2005), and (2) Jambon et al. (2008).

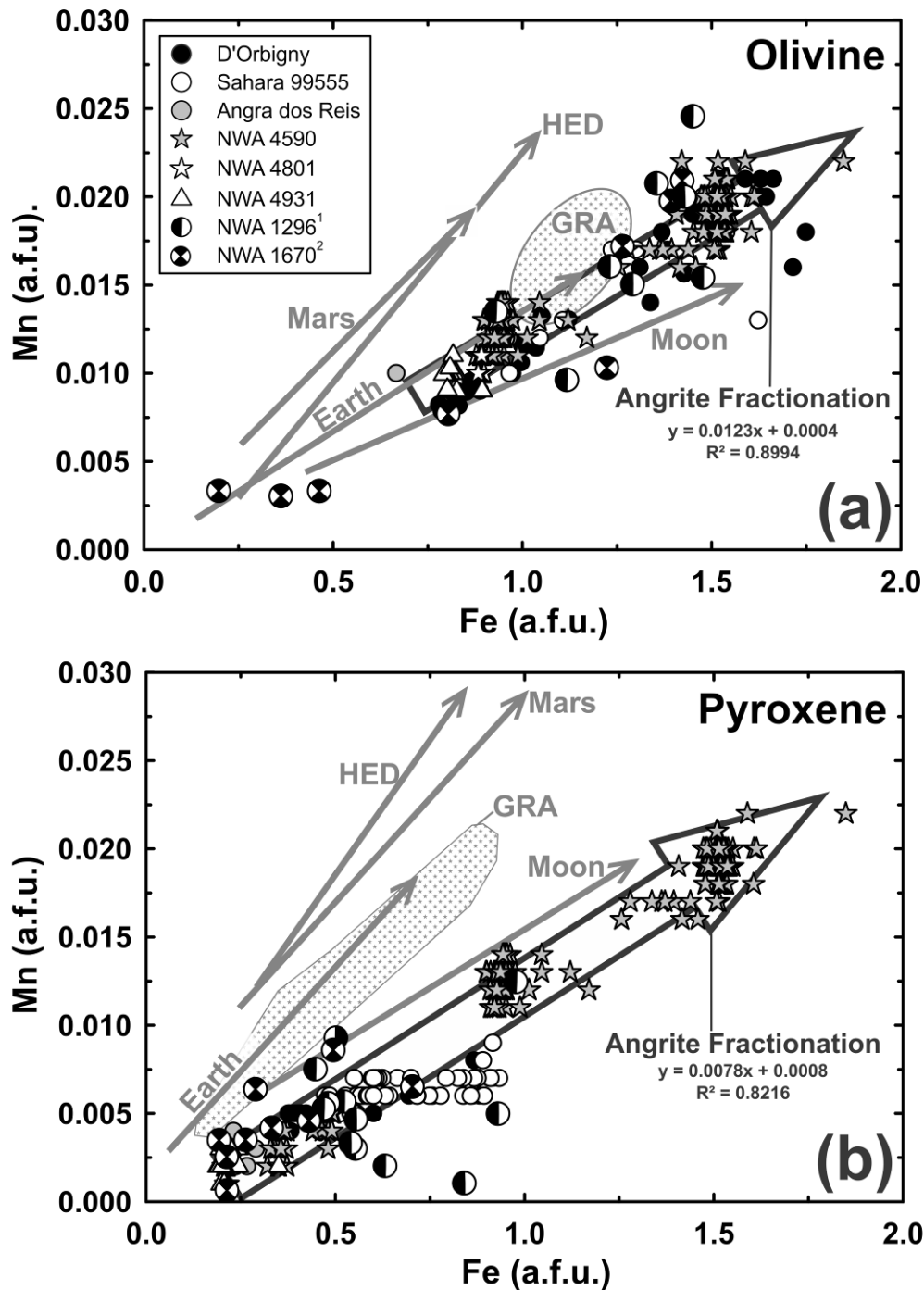


**Figure A4:** Iron and Mn abundances of olivines and pyroxenes. Olivine and pyroxene compositions of NWA 1296 and NWA 1670 were reported by (1) Jambon et al. (2005), and (2) Jambon et al. (2008). Fractionation trends for terrestrial, lunar, martian, howardite-eucrite-diogenite (HED) materials represent best-fit regressions after Fuhrman and Papike (1981), Karner et al. (2003, 2006), Mittlefehldt (1994), and Sack et al. (1991). Data for minerals of Graves Nunataks (GRA) 06128/9 were reported by Day et al. (2009) and Shearer et al. (2010).

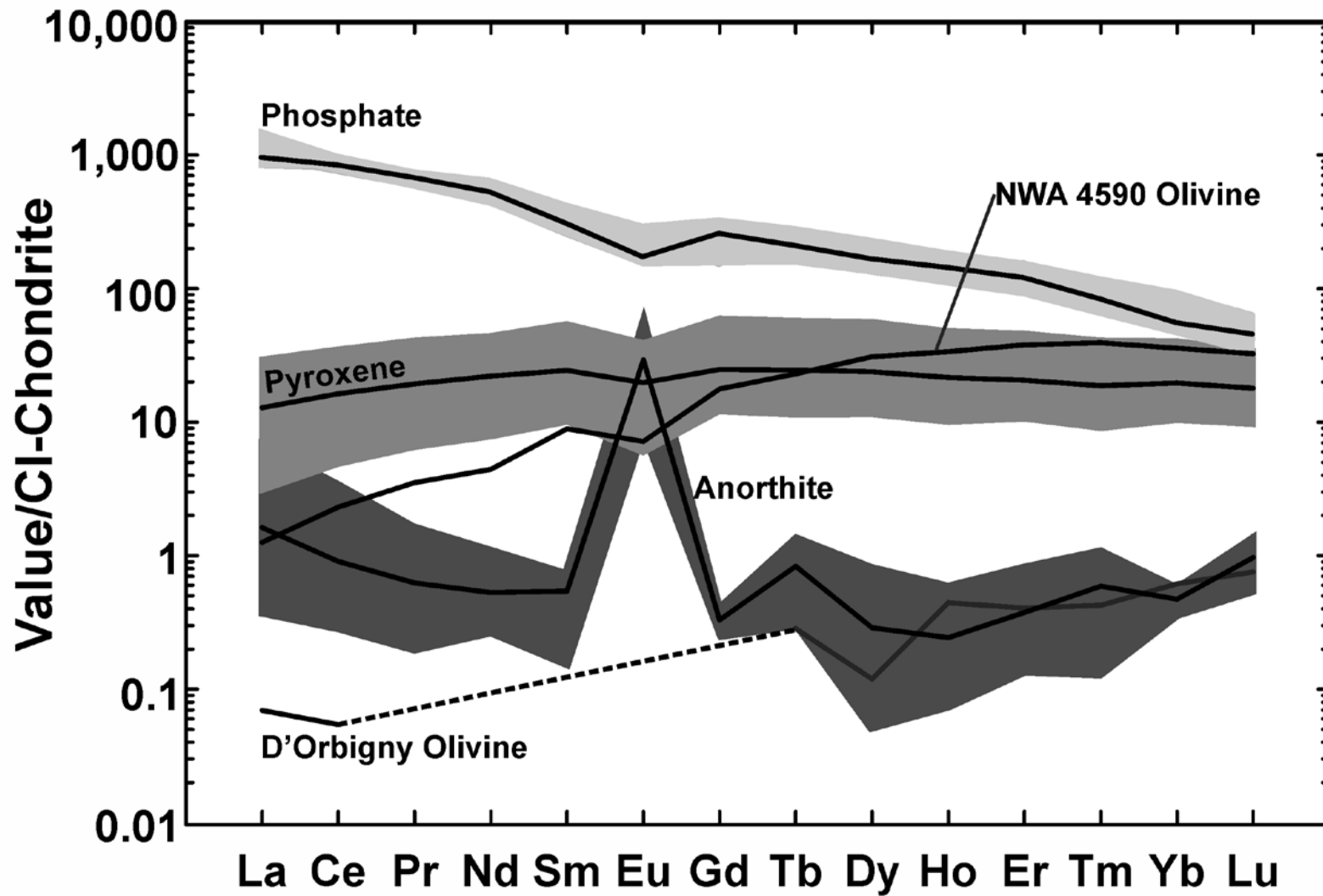


**Figure A5:** Average mineral rare-earth-element (REE) abundances in angrites (solid lines) normalized to the CI-chondrite estimate of Anders and Grevesse (1989). The gray fields delineate the range of mineral trace-element compositions determined in this study

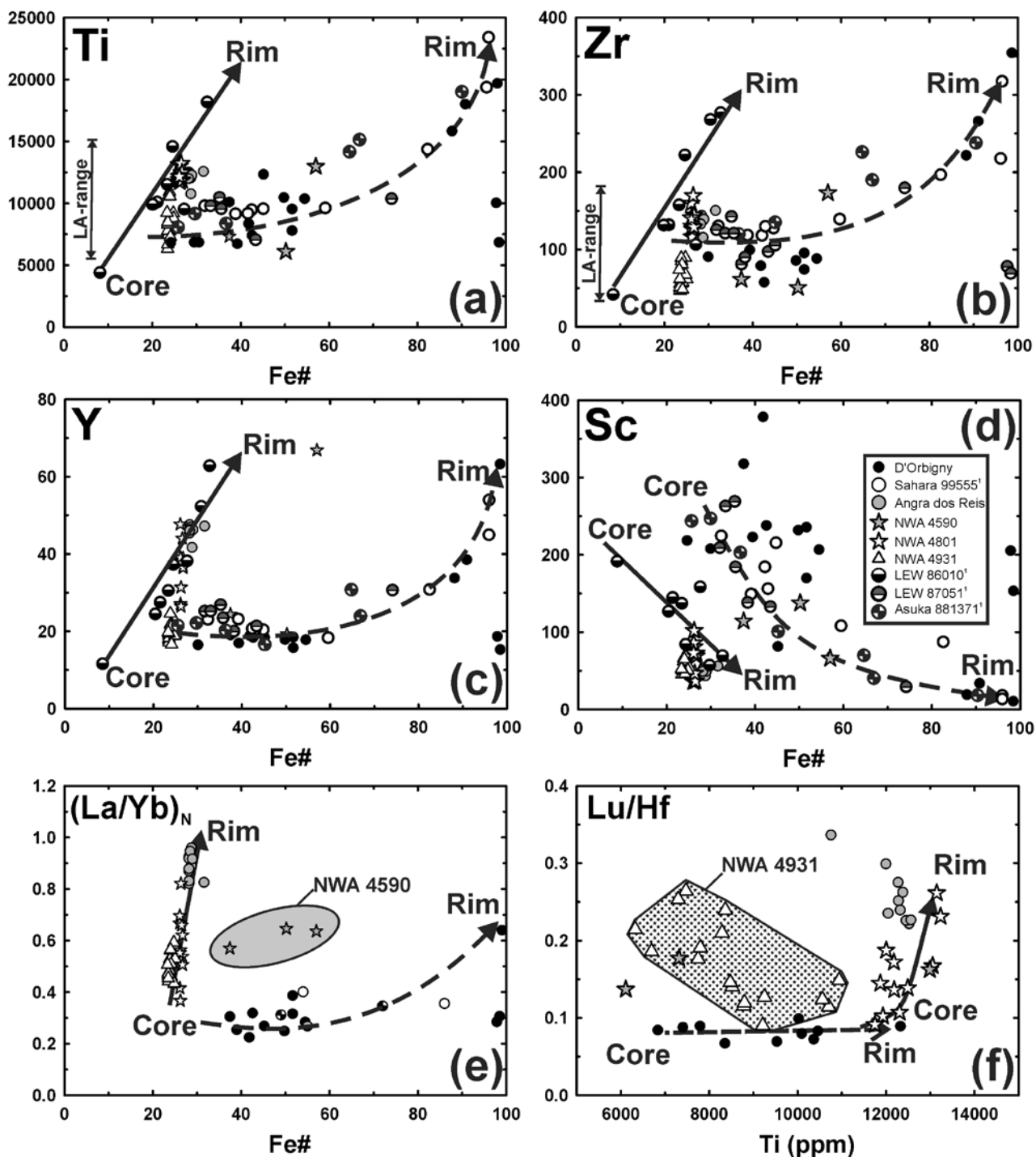


**Figure A6:** Trace- and minor-element abundances (ppm) and Fe# of angrite clinopyroxenes (where  $\text{Fe\#} = \text{Fe}/[\text{Mg} + \text{Fe}^{\text{total}}]$ ). <sup>1</sup>Ion-probe data (determined using a 5 to 25  $\mu\text{m}$  beam diameter) reported by Floss et al., 2003 are shown for comparison, and an arrow marks where laser-ablation values (generally determined with a 40-80  $\mu\text{m}$  beam) cover a more restricted range of trace-element abundances than ion-probe data. Arrows delineate core to rim variations of trace-element abundances and Fe#.

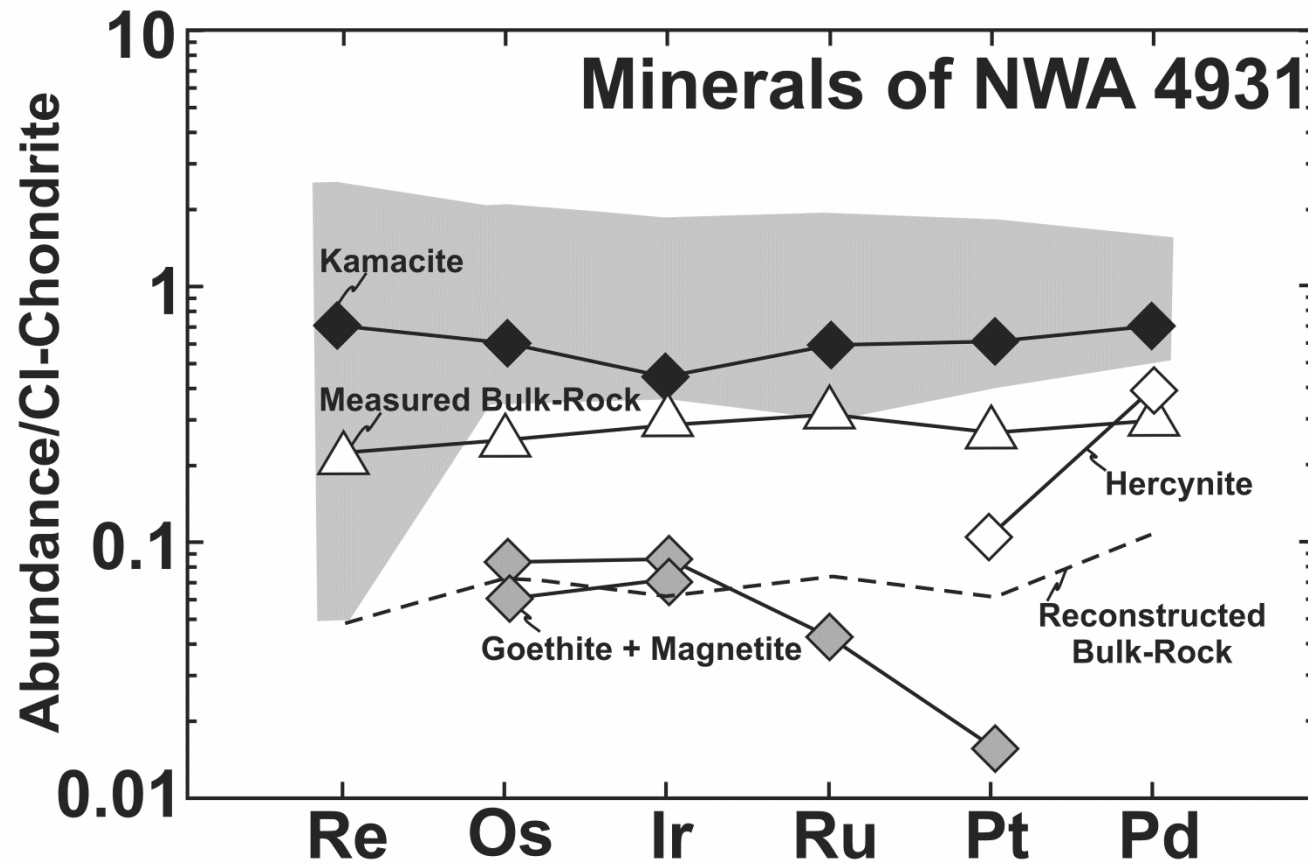


**Figure A7:** Highly-siderophile-element abundances of constituent minerals of NWA 4931 compared to measured and reconstructed bulk-rock compositions. The grey field marks the range of HSE concentrations measured in variably altered metal grains. All values are normalized to the HSE concentrations reported for Orgueil by Horan et al. (2003). The reconstructed bulk-rock composition is calculated from modal abundances (Table 1), and representative HSE concentrations determined by LA-ICP-MS. The difference between the reconstructed and measured bulk-rock HSE abundances reflects the heterogeneous distribution of HSE-carrier phases between the studied polished section and the bulk-rock powder fraction. Abundances of HSE in NWA 4931 occur in broadly chondritic proportions and are dominated by the HSE in metals thought to be of impact origin (Humayun et al., 2007).

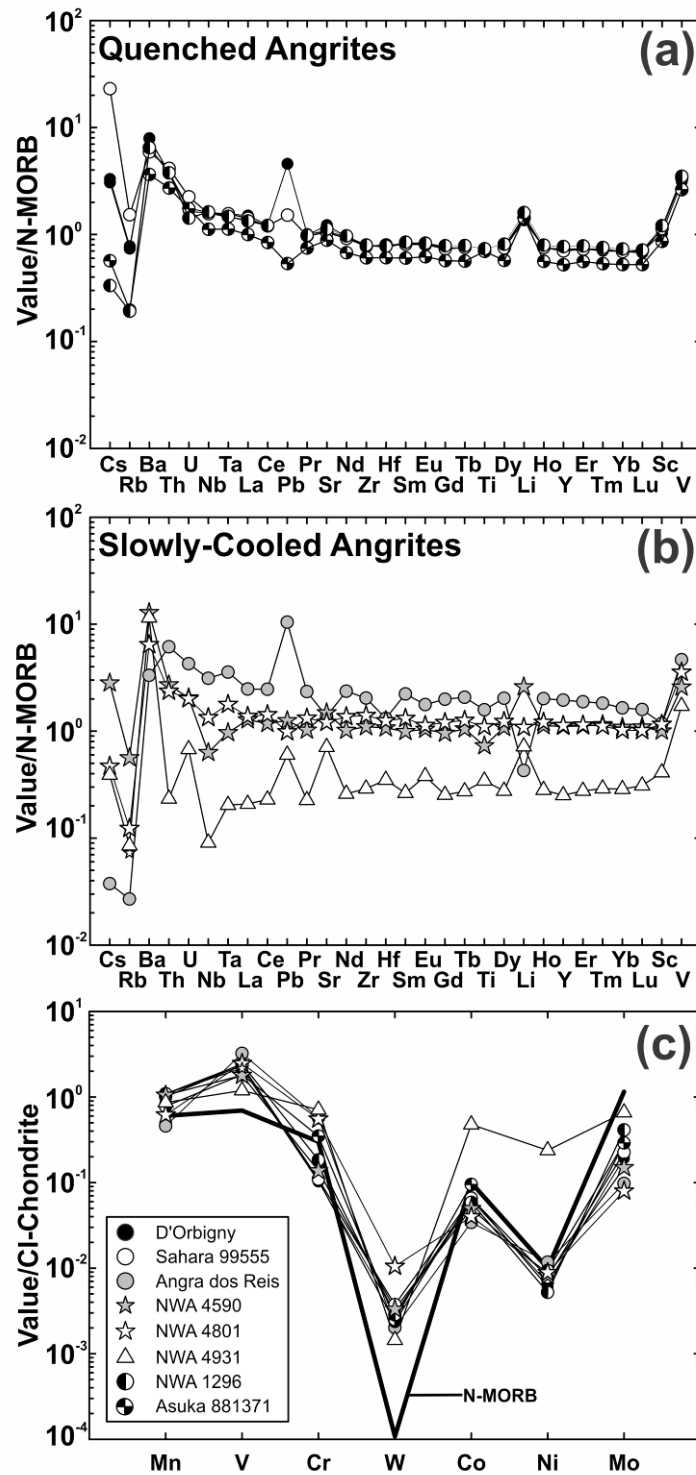


**Figure A8:** Extended trace- (a and b) and siderophile-element abundances (c) of angrite bulk-rock portions normalized to the N-MORB estimates of Newsom et al. (1986) and Sun and McDonough (1989).

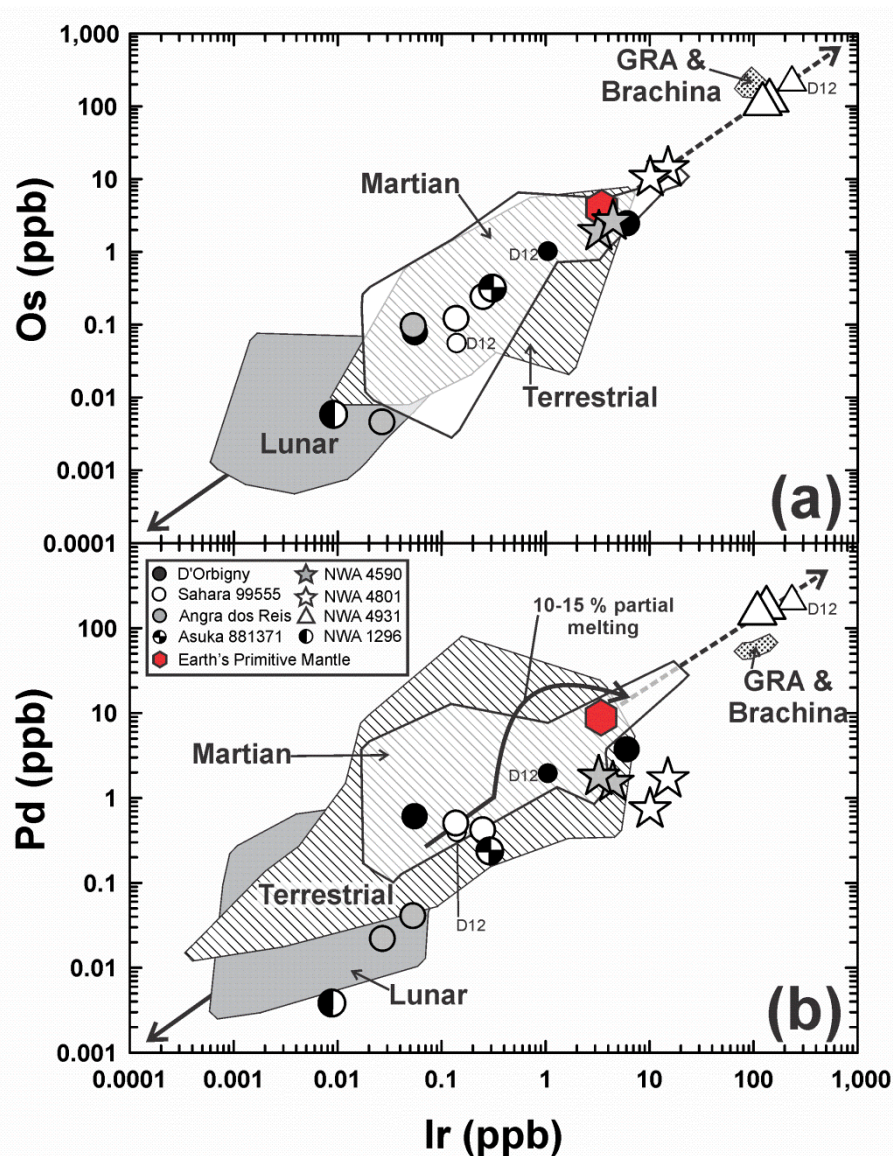
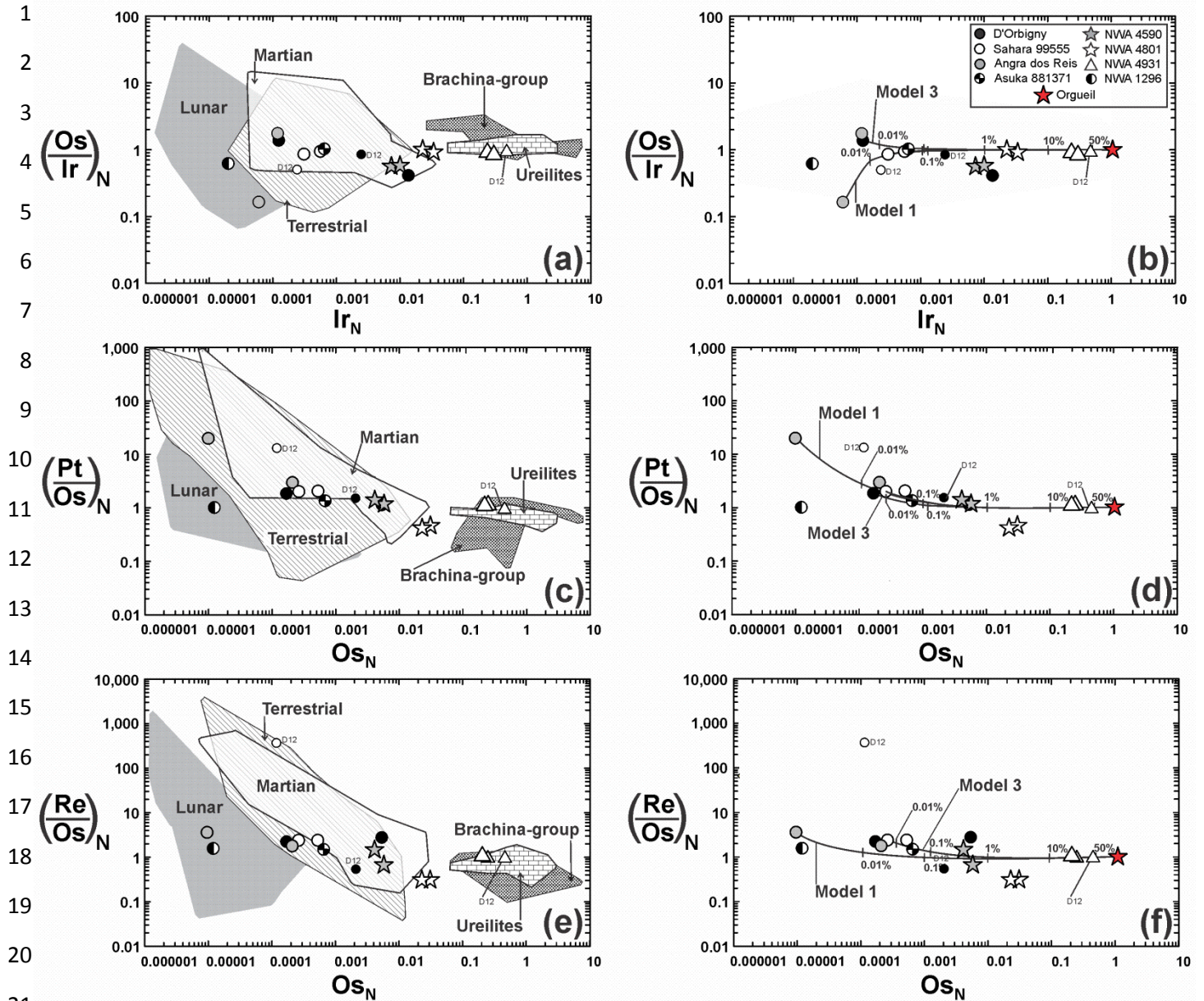
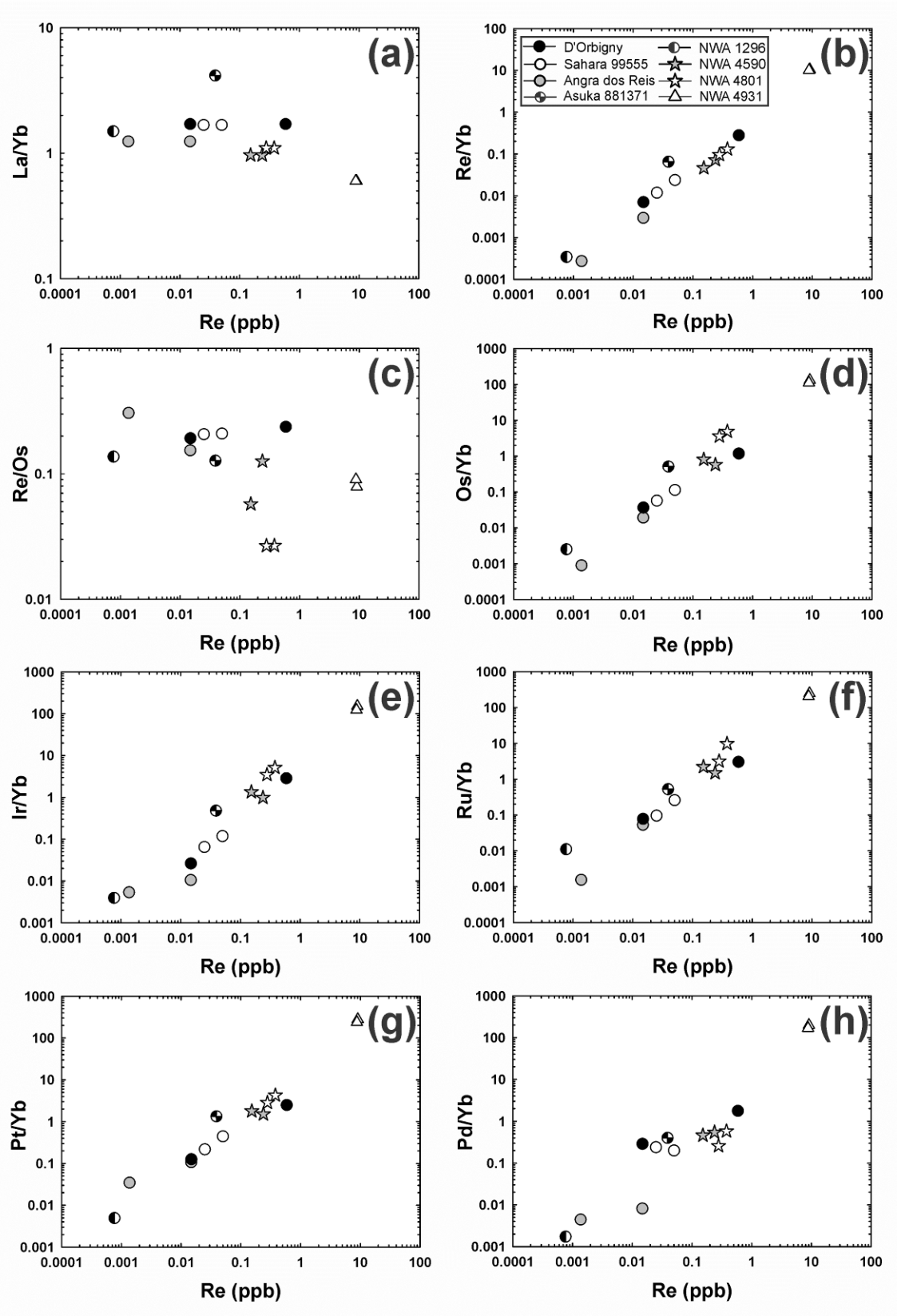


**Figure A9:** Abundances of Os, Ir, and Pd in portions of angrites, Graves Nunatak (GRA) 06128/9, brachina, and terrestrial, martian, and lunar samples. A broad 1:1 trend between Os and Ir reflects the similar compatibility of these two elements during partial melting and is supported by partial melting models (*c.f.*, Rehkämper et al., 1999 and references therein). In addition, Pd and Ir abundances of quenched angrites coincide with the field of lunar, terrestrial, and martian compositions. The curve that deviates from the broad 1:1 trend shown in (b) corresponds to Pd-Ir fractionation reported for terrestrial magmas thought to be generated at high-degrees of melting (10-15 %, assuming the melting model of Rehkämper et al., 1999). Data were sourced from Bézos et al. (2005), Brandon et al. (2000, 2012), Crocket (2000), Day et al. (2007, 2009, 2010a,b; 2012), Ireland et al. (2009), Luguet et al. (2007), Puchtel and Humayun (2000, 2005), Puchtel et al. (2004, 2005, 2008), Rehkämper et al. (1999), Riches et al. (2011) Walker et al. (2004), and Woodland et al. (2002). Data points labelled D12 correspond to those reported by Dale et al., 2012.



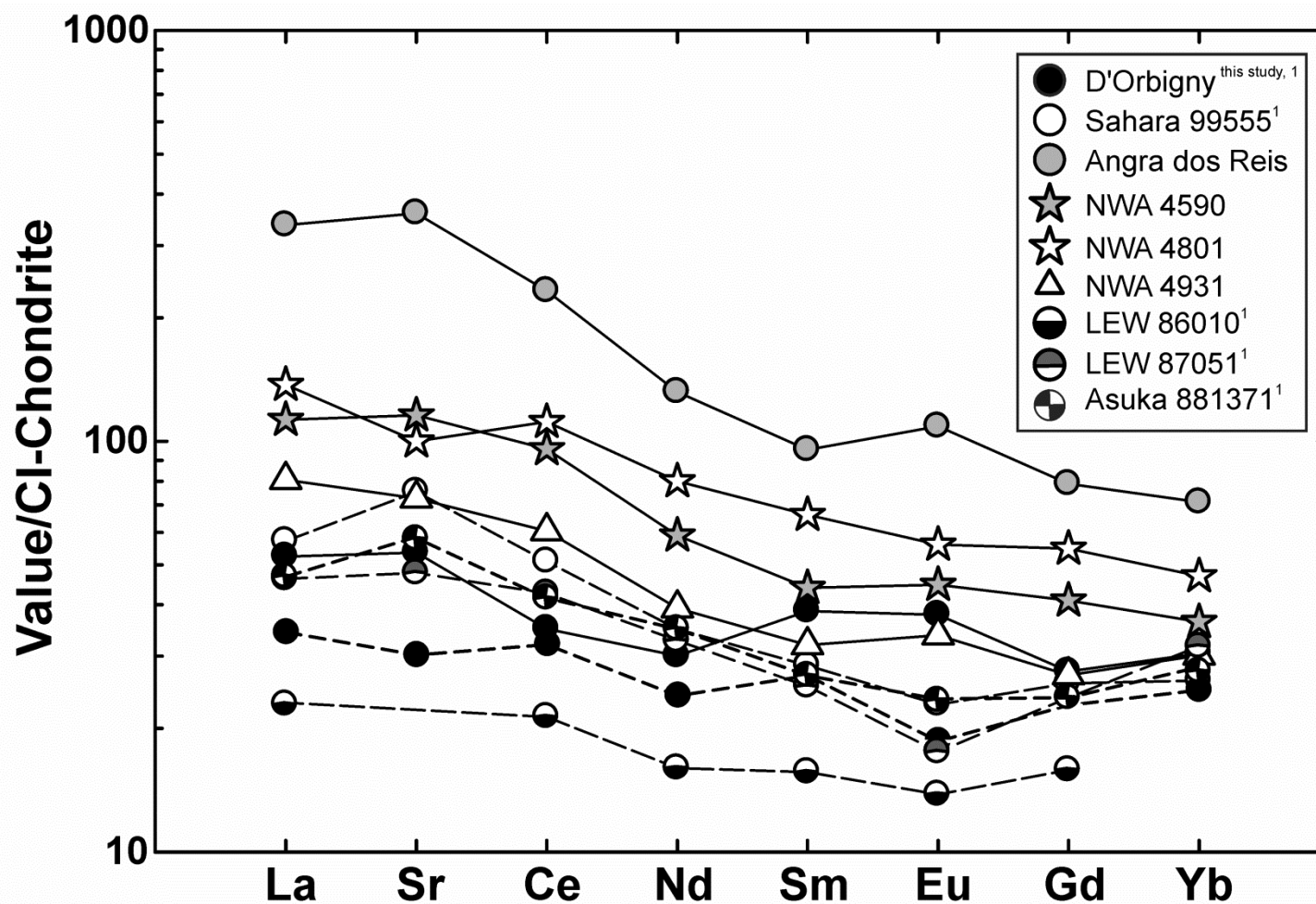
22 **Figure A10:** Highly-siderophile-element abundances and inter-element ratios normalised to the  
 23 composition of Orgueil (Horan et al., 2003). Lunar, terrestrial, martian, and ureilite data sources  
 24 include Bézos et al. (2005), Birck and Allègre (1994), Brandon et al. (2000, 2012), Crocket (2000), Day  
 25 et al. (2007, 2009, 2010a,b), Ireland et al. (2009), Luguet et al. (2007), Puchtel and Humayun (2000,  
 26 2005), Puchtel et al. (2004, 2005, 2008), Rankenburg et al. (2007, 2008), Rehkämper et al. (1999),  
 27 Riches et al. (2011), Walker et al. (2004), and Woodland et al. (2002). Brachina-group data  
 28 corresponds to brachina, GRA 06128 and 06129, and a selection of other brachinites and brachinite-like  
 29 achondrites studied by Day et al., 2012. Details of the mixing calculation are given in the main text.  
 30 Data points labelled D12 correspond to those reported by Dale et al., 2012.



31

32 **Figure A11:** Rhenium abundances compared to La- and HSE-values normalised to Yb-concentrations of the  
 33 studied angrites.





44

45 **Figure A13:** Melts in equilibrium with pyroxene core compositions (Appendix B) normalized to the CI-chondrite value of Anders and  
 46 Grevesse (1989). Melt compositions were calculated from average values of core compositions using the partition coefficients determined by  
 47 McKay et al., (1994). In general, abundances of  $\text{Al}_2\text{O}_3$  in pyroxene cores  $> 7$  wt. % (a  $550 \mu\text{m}$  crystal of D'Orbigny with a core  $\text{Al}_2\text{O}_3$   
 48 concentration of 4.64 wt. % is an exception, but the average  $\text{Al}_2\text{O}_3$  of core compositions for this sample is 6.26 wt. %. The 'lower'  
 49 representative clinopyroxene trace-element concentrations determined by 1 (where this symbol refers to the ion-probe study of Floss et al.,  
 50 2003) were used to calculate equilibrium melt compositions, and are delineated by dashed-lines.

51 **A3. Supplementary References**

- 52 Anand, M., Taylor, L. A., Floss, C., Neal, C. R., Terada, K., Tanikawa, S., 2006. Petrology and geochemistry of  
53 LaPaz Icefield 02205: A new unique low-Ti mare basalt meteorite. *Geochim. Cosmochim. Acta.*, 70(1), 246-  
54 264.
- 55 Anders, E., and Grevesse, N., 1989. Abundances of the elements - meteoritic and solar. *Geochim. Cosmochim. Acta*,  
56 53, 197-214.
- 57 Becker, H., Horan, M. F., Walker, R. J., Gao, S., Lorand, J-P., and Rudnick, R. L., 2006. Highly siderophile element  
58 composition of the Earth's primitive upper mantle: constraints from new data on peridotite massifs and  
59 xenoliths. *Geochim. Cosmochim. Acta*, 70, 4528-4550
- 60 Bézoz, A., Lorand, J-P., Humler, E., and Gros, M., 2005. Platinum-group element systematic in Mid-Oceanic Ridge  
61 basaltic glasses from the Pacific, Atlantic, and Indian Oceans. *Geochim. Cosmochim. Acta*, 69(10), 2613-2627.
- 62 Birck, J.-L., and Allègre, C. J., 1994. Contrasting Re/Os magmatic fractionation in planetary basalts. *Earth Planet.*  
63 *Sci. Lett.*, 124, 139-148.
- 64 Birck, J.-L., Roy-Barman, M., Capmas, F., 1997. Re-Os Isotopic Measurements at the Femtomole Level in Natural  
65 Samples. *Geostnd. Newslett.*, 21(1), 19-27.
- 66 Bischoff, A., Clayton, R. N., Makl, G., Mayeda T. K., Palme, H., Schultze, L., Srinivasan, G., Weber, H. W.,  
67 Weckwerth, G., and Wolf, D., 2000. Mineralogy, chemistry, noble gases, and oxygen- and magnesium-isotopic  
68 compositions of the angrite Sahara 99555. *Meteorit. Planet. Sci.*, 35, A27.
- 69 Boynton, W. V., Starzyk, P. M., and Schmitt, R. A., 1976. Chemical evidence for the genesis of the ureilites, the  
70 achondrite Chassigny and the nakhlites. *Geochim. Cosmochim. Acta*, 40(12), 1439-1447.
- 71 Brandon, A. D., Walker, R. J., Morgan, J. W., and Goles, G. G., 2000. Re-Os isotopic evidence for early  
72 differentiation of the Martian mantle. *Geochim. Cosmochim. Acta*, 64 (23), 4083-4095.
- 73 Brandon, A.D., Puchtel, I. S., Walker, R. J., Day, J. M. D., Irving, A. J., and Taylor, L. A., 2012. Evolution of the  
74 martian mantle inferred from  $^{187}\text{Re}$ - $^{187}\text{Os}$  isotope and highly siderophile element abundance systematics of  
75 shergottite meteorites. *Geochim. Cosmochim. Acta*, 76, 206-235.
- 76 Chen, C.Y., Frey, F.A., Garcia, M.O., Dalrymple, G.B., Hart, S.R., 1991. The tholeiite to alkali basalt transition at  
77 Haleakala volcano, Maui, Hawaii. *Contrib. Mineral. Petrol.* 106, 183-200.
- 78 Cohen, A. S., and Waters, F. G., 1996. Separation of osmium from geological materials by solvent extraction for  
79 analysis by thermal ionisation mass spectrometry. *Anal. Chim. Acta*, 332, 269-275.
- 80 Crocket, J.H., 2000. PGE in fresh basalt, hydrothermal alteration products, and volcanic incrustations of Kilauea  
81 volcano, Hawaii. *Geochim. Cosmochim. Acta*, 64(10), 1791-1807.
- 82 Dale, C. W., Burton, K. W., Greenwood, R. C., Gannoun, A., Wade, J., Wood, B. J., and Pearson, D. G., 2012. Late  
83 Accretion on the Earliest Planetesimals Revealed by the Highly Siderophile Elements. *Science*, 336, 72-75.
- 84 Day, J. M. D., Taylor, L. A., Floss, C., Patchen, A. D., Schnare, D. W., Pearson, D. G., 2006. Comparative  
85 petrology, geochemistry and petrogenesis of evolved, low-Ti lunar mare basalt meteorites from the La Paz  
86 icefield, Antarctica. *Geochim. Cosmochim. Acta*, 70, 1581-1600
- 87 Day, J. M. D., Pearson, D. G., and Taylor, L. A., 2007. Highly siderophile element constraints on accretion and  
88 differentiation of the Earth-Moon system. *Science*, 315, 217-219.
- 89 Day, J. M. D., Ash, R. D., Liu, Y., Bellucci, J. J., Rumble, D. III., McDonough, W. F., Walker, R. J., and Taylor, L.  
90 A., 2009. Early formation of evolved asteroidal crust. *Nature*, 457, 179-182.

- 91 Day, J. M. D., Walker, R. J., James, O. B., and Puchtel, I. S., 2010a. Osmium isotope and highly siderophile element  
92 systematics of the lunar crust. *Earth and Planetary Science Letters* 289, 595-605.
- 93 Day, J. M. D., Pearson, D. G., MacPherson, C. G., Lowry, D., and Carrecedo, J.-C., 2010b. Evidence for distinct  
94 proportions of oceanic crust and lithosphere in HIMU-type mantle beneath El Hierro and La Palma, Canary  
95 Islands. *Geochim. Cosmochim. Acta*, 74, 6565-6589.
- 96 Day, J. M. D., Walker, R. J., Ash, R. D., Liu, Y., Rumble, D., Irving, A. J., Goodrich, C. A., Tait, K., McDonough,  
97 W. F., Taylor, L. A., 2012. Origin of felsic achondrites Graves Nunatak 06128 and 06129, and ultramafic  
98 brachinites and brachinite-like achondrites by partial melting of volatile-rich primitive parent bodies. *Geochim.*  
99 *Cosmochim. Acta*, 81, 94-128.
- 100 Floss, C., Crozaz, G., McKay, G., Mikouchi, T., and Killgore, M., 2003. Petrogenesis of angrites. *Geochim.*  
101 *Cosmochim. Acta*, 67(24), 4775-4789.
- 102 Fuhrman, M., and Papike, J. J., 1981. Howardites and polymict eucrites: Regolith samples from the eucrite parent  
103 body. *Petrology of Bholgati, Bununu, Kapoeta, and ALHA 76005. Proc. of Lunar Planet. Sci. Conf.*, 12B, 1257-  
104 1279.
- 105 Garcia, M.O., Foss, D.J.P., West, H.B., Mahoney, J.J., 1995. Geochemical and isotopic evolution of Loihi Volcano,  
106 Hawaii. *J. Petrol.* 36, 1647-1674.
- 107 GEOREM, <http://georem.mpch-mainz.gwdg.de>
- 108 Goodrich, C. A., Herd, C. D. K., and Taylor, L. A., 2003. Spinels and oxygen fugacity in olivine-phyric and  
109 ilherzolithic shergottites. *Meteorit. Planet. Sci.*, 38(12), 1773-1792.
- 110 Greenwood, R. C., Franchi, I. A., Jambon, A., and Buchanan, P C., 2005. Widespread magma oceans on asteroidal  
111 bodies in the early Solar System. *Nature*, 435, 916-918.
- 112 Günther, D., and Heinrich, C. A., 1999, Enhanced sensitivity in laser ablation-ICP mass spectrometry using helium-  
113 argon mixtures as aerosol carrier. *J. Anal. At. Spectrom.*, 14, 1363-1368.
- 114 Gurriet, P.C. 1988, *Geochemistry of Hawaiian dredged lavas*. MSc Thesis, Massachusetts Institute of Technology.
- 115 Herd, C. D. K., 2006. Insights into the redox history of the NWA 1068/1110 martian basalt from mineral equilibria  
116 and vanadium oxybarometry. *Amer. Min.*, 91(10), 1616-1627.
- 117 Horan, M. F., Walker, R. J., Morgan, J. W., Grossman, J. N., and Rubin, A., 2003. Highly siderophile elements in  
118 chondrites. *Chem. Geol.*, 196, 5-20.
- 119 Humayun, M., Irving, A. J., and Kuehner, S. M., 2007. Siderophile elements in metal-rich angrite NWA 2999.  
120 *Lunar Planet. Sci. Conf.*, abstract #1221.
- 121 Ireland, T. J., Walker, R. J., and Garcia, M. O., 2009. Highly siderophile element and <sup>187</sup>Os isotope systematic of  
122 Hawaiian picrites: Implications for parent melt composition and source heterogeneity. *Chem. Geol.*, 260(1-2),  
123 112-128.
- 124 Irving, A.J., Kuehner, S.M., Rumble, D., Bunch, T.E., and Wittke, J.H., 2005. Unique Angrite NWA 2999: The  
125 Case for Samples from Mercury. *Amer. Geophys. Union Fall Meeting*, abstract #P51A-0898.
- 126 Irving, A.J., Kuehner, S.M, and Rumble, D., 2006. A Fresh Plutonic Igneous Angrite Containing Grain Boundary  
127 Glass From Tammassint, Northwest Africa. *Amer. Geophys. Union Fall Meeting*, abstract #P51E-1245.
- 128 Jambon, A., Barrat, J.-A., Boudouma, O., Fonteilles, M., Badia, D., Göpel, C., and Bohn, M., 2005. Mineralogy and  
129 petrology of the angrite Northwest Africa 1296. *Meteorit. Planet. Sci.*, 40(3), 361-375.
- 130 Jambon, A., Boudouma, O., Fonteilles, M., Le Guillou, C., Badia, D., and Barrat, J.-A. 2008. Petrology and  
131 mineralogy of the angrite Northwest Africa 1670. *Meteorit. Planet. Sci.*, 43(11), 1783-1795.

- 132 Jochum K. P., Stoll B., Herwig K., Willbold M., Hofmann A. W., Amini M., Liu Dun-Yi, Abouchami W.,  
133 Hellebrand E., Mocek B., Raczek I., Stracke A., Alard O., Bouman C., Becker S., Dücking M., Brätz H., Klemm  
134 R., de Bruin D., Canil D., Cornell D., De Hoog J. C. M., Dalpé C., Danyushevsky L. V., Eisenhauer A., Gao Y.,  
135 Snow J. E., Groschopf N., Günther D., Latkoczy C., Guillong M., Hauri E. H., Höfer H. E., Lahaye Y., Horz K.,  
136 Jacob D. E., Kasemann S., Kent A. J. R., Zack T., Ludwig T., Mason P. R. D., Meixner A., Rosner M., Misawa  
137 K., Nash B. P., Pfänder J. A., Premo W. R., Weidong D. S., Tiepolo M., Vannucci R., Vennemann T. W.,  
138 Wayne D., and Woodhead J. D., 2006. MPI-DING reference glasses for in-situ microanalyses: New reference  
139 values for element concentrations and isotope ratios. *Geochem. Geophys. Geosyst.*, 7,  
140 doi:10.1029/2005GC00106.
- 141 Johnson, J. E., Scrymgour, J. M., Jarosewich, E., Mason, B., 1977. Brachina meteorite – a chassignite from South  
142 Australia. *Rec. S. Austral. Mus.*, 17, 309–319.
- 143 Joy, K. H., Crawford, I. A., Downes, H., Russell, S. S., Kearsley, A. T., 2006. A petrological, mineralogical, and  
144 chemical analysis of the lunar mare basalt meteorite LaPaz Icefield 02205, 02224, 02226. *Meteorit. Planet. Sci.*,  
145 41(7), 1003-1025.
- 146 Karner, J. M., Papike, J. J., and Shearer, C. K., 2003. Olivine from planetary basalts: chemical signatures that  
147 indicate planetary parentage and those that record igneous settings and processes, *Am. Mineral.*, 88, 806-816.
- 148 Karner, J. M., Papike, J. J., and Shearer, C. K., 2006. Comparative planetary mineralogy: Pyroxene major- and  
149 minor-element chemistry and partitioning of vanadium between pyroxene and melt in planetary basalts. *Am.*  
150 *Mineral.*, 91, 1574-1582.
- 151 Kuehner, S.M., Irving, A.J., Bunch, T.E., Wittke, J.H., Hupé, G.M., and Hupé, A.C., 2006. Coronas and  
152 Symplectites in Plutonic Angrite NWA 2999 and Implications for Mercury as the Angrite Parent Body. 39<sup>th</sup>  
153 Lunar Planet. Sci. Conf., abstract #1344.
- 154 Luguét, A., Shirey, S. B., Lorand, J.-P., Horan, M. F., and Carlson, R. W., 2007. Residual platinum-group minerals  
155 from highly depleted harzburgites of the Lherz massif (France) and their role in HSE fractionation of the  
156 mantle. *Geochim. Cosmochim. Acta*, 71, 3082-3097
- 157 Lunar sample compendium, Meyer, C., 2012, <http://curator.jsc.nasa.gov/lunar/compendium.cfm>
- 158 Mars meteorite compendium, Meyer, C., 2012; <http://curator.jsc.nasa.gov/antmet/mmc/>
- 159 McCubbin, F. M., Riner, M. A., Vander Kaaden, K. E., and Burkemper, L. K., 2012. Is Mercury a volatile-rich  
160 planet? *Geophys. Res. Lett.*, 39, L09202, doi:10.1029/2012GL051711.
- 161 McDonough, W. F., and Sun, S.-s., 1995. The composition of the Earth. *Chem. Geol.*, 120, 223-254.
- 162 McKay, G., Le L., Wagstaff, J., and Crozaz, G., 1994. Experimental partitioning of rare earth elements and  
163 strontium: Constraints on petrogenesis and redox conditions during crystallization of Antarctic angrite Lewis  
164 Cliff 86010. *Geochim. Cosmochim. Acta*, 58(13), 2911-2919.
- 165 Mittlefehldt, D. W., 1994. The genesis of diogenites and HED parent body petrogenesis. *Geochim. Cosmochim.*  
166 *Acta*, 58(5), 1537-1552.
- 167 Mittlefehldt, D. W., Bogard, D. D., Berkley, J. L., & Garrison, D. H., 2003. Brachinites: Igneous rocks from a  
168 differentiated asteroid. *Meteorit. Planet. Sci.*, 38(11), 1601-1625.
- 169 Newsom, H. W., White, W. M., Jochum, K. P., and Hofmann, A. W., 1986. Siderophile and chalcophile element  
170 abundances in oceanic basalts, Pb isotope evolution and growth of the Earth's core. *Earth Planet. Sci. Lett.*,  
171 80(3-4), 299-313.
- 172 Nier, A. O., 1950. The isotopic constitution of oxygen. *Phys. Rev.*, 52, 885.
- 173 Norman, M. D., and Garcia, M. O., 1999. Primitive magmas and source characteristics of the Hawaiian plume:  
174 petrology and geochemistry of shield picrites. *Earth planet. Sci. Lett.*, 168, 27-44.

- 175 Puchtel, I. S., and Humayun, M., 2000. Platinum group elements in Kostomuksha komatiites and basalts:  
176 Implications for oceanic crust recycling and core-mantle interaction. *Geochim. Cosmochim. Acta*, 64(24),  
177 4227-4242.
- 178 Puchtel, I. S., and Humayun, M., 2005. Highly siderophile element geochemistry of <sup>187</sup>Os-enriched 2.8Ga  
179 Kostomuksha komatiites, Baltic Shield. *Geochim. Cosmochim. Acta*, 69(6), 1607-1618.
- 180 Puchtel, I. S., Brandon, A. D., and Humayun, M., 2004. Precise Pt-Re-Os isotope systematic of the mantle from 2.7  
181 Ga komatiites. *Earth Planet. Sci. Lett.*, 224, 157-174.
- 182 Puchtel, I. S., Brandon, A. D., Humayun, M., and Walker, R. J., 2005. Evidence for the early differentiation of the  
183 core from Pt-Re-Os isotope systematic of 2.8 Ga komatiites. *Earth Planet. Sci. Lett.*, 237, 118-134
- 184 Puchtel, I. S., Walker, R. J., James, O. B., and Kring, D. A., 2008. Osmium isotope and highly siderophile element  
185 systematic of lunar impact melt breccias: implications for the late accretion history of the Moon and Earth.  
186 *Geochim. Cosmochim. Acta*, 72, 3022-3042.
- 187 Rankenburg, K., Brandon, A. D., and Humayun, M., 2007, Osmium isotope systematics of ureilites. *Geochim.*  
188 *Cosmochim. Acta.*, 71, 2402-2413.
- 189 Rankenburg, K., Humayun, M., Brandon, A. D., and Herrin, J. S., 2008. Highly siderophile elements in ureilites.  
190 *Geochim. Cosmochim. Acta.*, 72, 4642-4659.
- 191 Rehkämper, M., Halliday, A. N., Fitton, J. G., Lee, D.-C., Wieneke, M., and Arndt, N. T., 1999. Ir, Ru, Pt, and Pd in  
192 basalts and komatiites: New constraints for the geochemical behaviour of the platinum-group elements in the  
193 mantle. *Geochim. Cosmochim. Acta*, 63(22), 3915-3934.
- 194 Rhodes, J. M., 1996. Geochemical stratigraphy of lava flows sampled by the Hawaii scientific drilling project. *J.*  
195 *Geophys. Res.* 101, 11729-11746.
- 196 Rhodes, J. M., and Villinger M. J., 2004. Composition of basaltic lavas sampled by phase-2 of the Hawaii scientific  
197 drilling project: geochemical stratigraphy and magma types. *Geochem. Geophys. Geosyst.*, 5, 1-38.
- 198 Riches A.J.V., Liu Y., Day J.M.D., Puchtel I. S., Rumble D., McSween H.Y., Walker R.J., and Taylor L.A., 2011.  
199 Petrology and Geochemistry of Yamato 984028: A Cumulate Lherzolithic Shergottite with Affinities to Y  
200 000027, Y000047, and Y 000097. *Polar Sci.*, 4(4), 497-514.
- 201 Sack, R. O., Azeredo, W. J., and Lipschutz, M. E., 1991. Olivine diogenites: the mantle of the eucrite parent body.  
202 *Geochim. Cosmochim. Acta*, 55(4), 1111-1120.
- 203 Shearer, C. K., Burger, P. V., Neal, C. R., Sharp, Z., Spivak-Birndorf, L., Borg, L., Fernandes, V. A., Papike, J. J.,  
204 Karner, J., Wadhwa, M., Gaffney, A., Shafer, J., Geissman, J., Atudorei, N. V., Herd, C. K., Weiss, B. P., King,  
205 P. L., Crowther, S. A., and Gilmour, J. D., 2010. Non-basaltic asteroidal magmatism during the earliest stages  
206 of solar system evolution: A view from Antarctic achondrites Graves Nunatak 06128 and 06129, *Geochim.*  
207 *Cosmochim. Acta*, 74(3), 1172-1199.
- 208 Shirey, S. B., and Walker, R. J., 1998. The Re-Os isotope system in cosmochemistry and high-temperature  
209 geochemistry. *Annu. Rev. Earth Planet. Sci.*, 26, 423-500.
- 210 Simonetti, A., Buzon, M. R., and Creaser, R. A., 2008. In-situ elemental and Sr isotope investigation of human tooth  
211 enamel by laser ablation-MC-ICP-MS: Successes and pitfalls. *Archaeometry*, 50(2), 371-385.
- 212 Sun, S.-s., and McDonough, W. F., 1989. Chemical and Isotopic Systematics of Oceanic Basalts: Implications for  
213 Mantle Composition and Processes, In: *Magmatism in the Ocean Basins*, Saunders A.D., and Norry M.J. (Eds.),  
214 *Spec. Publ. Geol. Soc. Lond.* , No. 42, 313-345.
- 215 Tanaka, R., Nakamura, E., Takahashi, E., 2002. Geochemical evolution of Koolau volcano, Hawaii. In: Takahashi,  
216 E., Lipman, P.W., Garcia, M.O., Naka, J., Aramaki, S. (Eds.), *Hawaiian Volcanoes; Deep Underwater*  
217 *Perspectives*. American Geophysical Union, Washington, DC, United States, pp. 311-332.

- 218 Walker, R. J., Horan, M. F., Shearer, C. K., and Papike, J. J., 2004. Low abundances of highly siderophile elements  
219 in the lunar mantle: evidence for prolonged late accretion. *Earth Planet. Sci. Lett.*, 244, 399-413.
- 220 Wang, K., Moynier, F., Dauphas, N., Barrat, J.-A., Craddock, P., and Sio, C. K., 2012. Iron isotope fractionation in  
221 planetary crusts. *Geochim. Cosmochim. Acta.*, 89, 31-45.
- 222 Wasserburg, G. J., Tera, F., Papanastassiou, D. A., and Huneke, J. C., 1977. Isotopic and chemical investigations on  
223 Angra dos Reis. *Earth Planet., Sci.* 35, 294-316.
- 224 Weider, S. Z., Nittler, L. R., Starr, R. D., McCoy, T. J., Boynton, W. V., Ebel, D. S., Ernst, C. M., Evans, L. G.,  
225 Goldsten, J. O., Hamara, D. K., Lawrence, D. J., McNutt, R. L., Schlemm C. E., Solomon, S. C., and Sprague,  
226 A. L., 2011. Major-element composition of Mercury's surface from MESSENGER X-ray Spectrometry. 2011  
227 AGU Fall Meeting, abstract # P43E-04.
- 228 West, H.B., Garcia, M.O., Gerlach, D.C., Romano, J., 1992. Geochemistry of tholeiites from Lanai, Hawaii.  
229 *Contrib. Mineral. Petrol.* 112, 520-542.
- 230 Woodland, S. J., Pearson, D. G., and Thirlwall, M. F., 2002. A platinum group element and Re-Os isotope  
231 investigation of siderophile element recycling in subduction zones: Comparison of Grenada, Lesser Antilles  
232 Arc, and the Izu-Bonin Arc. *Journal of Petrology*, 43(1), 171-198.
- 233 Zolotov, M. Y., Sprague, A. L., Nittler, L. R., Weider, S. Z., Starr, R. D., Evans, L. G., Boynton, W. V., Goldsten, J.  
234 O., Hauck, S. A., and Solomon, S. C., 2011. Implications of the MESSENGER of high sulfur abundance on the  
235 surface of mercury. 2011 AGU Fall Meeting, abstract # P41A-1584.
- 236 Zhang, J., Dauphas, N., Davis A. M., Leya, I., Fedkin, A., 2012. The proto-Earth as a significant source of lunar  
237 material. *Nature Geosci.*, 5, 251-255.

238

239

240

-end--

241